nature nanotechnology

SUPPLEMENTARY INFORMATION

https://doi.org/10.1038/s41565-020-0696-3

In the format provided by the authors and unedited.

Subretinally injected semiconducting polymer nanoparticles rescue vision in a rat model of retinal dystrophy

José Fernando Maya-Vetencourt[1,2,3], Giovanni Manfredi[4], Maurizio Mete[5], Elisabetta Colombo[1,2], Mattia Bramini[1,12], Stefano Di Marco[1,2], Dmytro Shmal[1], Giulia Mantero[1], Michele Dipalo[6], Anna Rocchi[1,2], Mattia L. DiFrancesco[1], Ermanno D. Papaleo[1], Angela Russo[5], Jonathan Barsotti[4], Cyril Eleftheriou[1,13], Francesca Di Maria[7], Vanessa Cossu[2,8], Fabio Piazza[9], Laura Emionite[2], Flavia Ticconi[2,8,14], Cecilia Marini[10], Gianmario Sambuceti[2,8], Grazia Pertile[5], Guglielmo Lanzani[4,11] ✉ and Fabio Benfenati[1,2] ✉

[1]Centre for Synaptic Neuroscience and Technology, Istituto Italiano di Tecnologia, Genoa, Italy. [2]IRCCS Ospedale Policlinico San Martino, Genoa, Italy. [3]Department of Biology, University of Pisa, Pisa, Italy. [4]Centre for Nano Science and Technology, Istituto Italiano di Tecnologia, Milan, Italy. [5]Ophthalmology Department, IRCCS Ospedale Sacro Cuore Don Calabria, Negrar, Italy. [6]Plasmon Nanotechnologies, Istituto Italiano di Tecnologia, Genoa, Italy. [7]CNR Institute of Organic Synthesis and Photoreactivity (ISOF), Bologna, Italy. [8]Department of Health Science, Nuclear Medicine, University of Genoa, Genoa, Italy. [9]ENT Department, ASST Mantova, Mantua, Italy. [10]CNR Institute of Bioimages and Molecular Physiology, Milan (Genoa Section), Genoa, Italy. [11]Department of Physics, Politecnico di Milano, Milan, Italy. [12]Present address: Department of Applied Physics, University of Granada, Granada, Spain. [13]Present address: Departments of Ophthalmology and Neurology, Weil Medical College of Cornell University, White Plains, NY, USA. [14]Present address: Department of Oncohematology, Nuclear Medicine Unit, Faenza Hospital, Faenza, Italy. ✉e-mail: guglielmo.lanzani@iit.it; fabio.benfenati@iit.it

SUBRETINALLY INJECTED SEMICONDUCTING POLYMER NANOPARTICLES RESCUE VISION IN A RAT MODEL OF RETINAL DYSTROPHY

José Fernando Maya-Vetencourt, Giovanni Manfredi, Maurizio Mete, Elisabetta Colombo[1], Mattia Bramini, Stefano Di Marco, Dmytro Shmal, Giulia Mantero, Michele Dipalo, Anna Rocchi, Mattia L. DiFrancesco, Ermanno D. Papaleo, Angela Russo, Jonathan Barsotti, Cyril Eleftheriou, Francesca Di Maria, Vanessa Cossu, Fabio Piazza, Laura Emionite, Flavia Ticconi, Cecilia Marini, Gianmario Sambuceti, Grazia Pertile, Guglielmo Lanzani, Fabio Benfenati

SUPPLEMENTARY INFORMATION

SUPPLEMENTARY TEXT

Photothermal effects at the nanoparticle-cell interface

The Fourier law in radial symmetry describes the thermal equilibrium of a single nanoparticle (NP) embedded in water and under constant illumination:

$$\frac{\Delta Q}{\Delta t} = -k\frac{\Delta T}{\Delta r}S(r) \qquad \text{eq. 1}$$

where $\frac{\Delta Q}{\Delta t}$ is the power input, k is the thermal conductivity of water (*0.6 W/mK*), *r* is the distance from NP centre and *S(r)* a spherical surface centred on the NP. Equation 1 describes the IN-OUT energy balance in steady state. The temperature profile is:

$$\Delta T(x) = \frac{I_0 R_{NP}^2}{4k(R_{NP}+x)} \qquad \text{eq. 2}$$

where I_0 is the light intensity, $R_{np}$is the NP radius and x is the radial distance from the NP surface. At the NP surface (*x=0*)

$$\Delta T = \frac{I_0 R_{NP}}{4k} \qquad \text{eq. 3}$$

The average light intensity impinging onto the explanted retinas is about $I_0 = 50\ \mathrm{mW/mm^2}$. Plugging this numerical value into eq.3 and using $R_{NP} = 200\ nm,$ we get $\Delta T = 5\ mK$. Accordingly, the expected cell membrane capacity variation by using the thermal coefficient $\alpha = 0.003\ K^{-1}$, is $\Delta C/C = \alpha\Delta T = 1.5 \times 10^{-5}$ [S1]. In turn, the relative change in membrane potential is only 1.5×10^{-5}.

Such result is valid in the case of a single isolated NP. We have indication that clustering is occurring in the biological environment (see **Fig. 2**) with an average cluster volume of 10 μm^3. Assuming a cluster is a large particle of radius ~1 μm, the corresponding heating would be 25 mK, still way out significance. To account for many NPs dispersed in a medium, we considered a distribution of P3HT-NPs inside a high-density polyethylene (HDPE) film, with a NP concentration of 0.2 ± 0.1 NPs/μm^3. We then measured the temperature changes in the proximity (few μm) of the film surface in contact with a saline bath by using the technique reported in [S2].

The figure (*panel **a**)* shows the experimental results shining the interface with green light at 96 mW/mm^2 and for various illumination times. The maximum rise in temperature is about 6 K. However, when measuring explanted retinas, the NP concentration is 3 orders of magnitude smaller, around (3 ± 0.09) x 10^{-4} NPs/μm^3. The latter value comes from counting the number of NPs per volume fraction in confocal fluorescence images of *ex vivo* samples (*panel **b***). The temperature rise, that is linear with the NP concentration, is thus negligibly small, in the mK range.

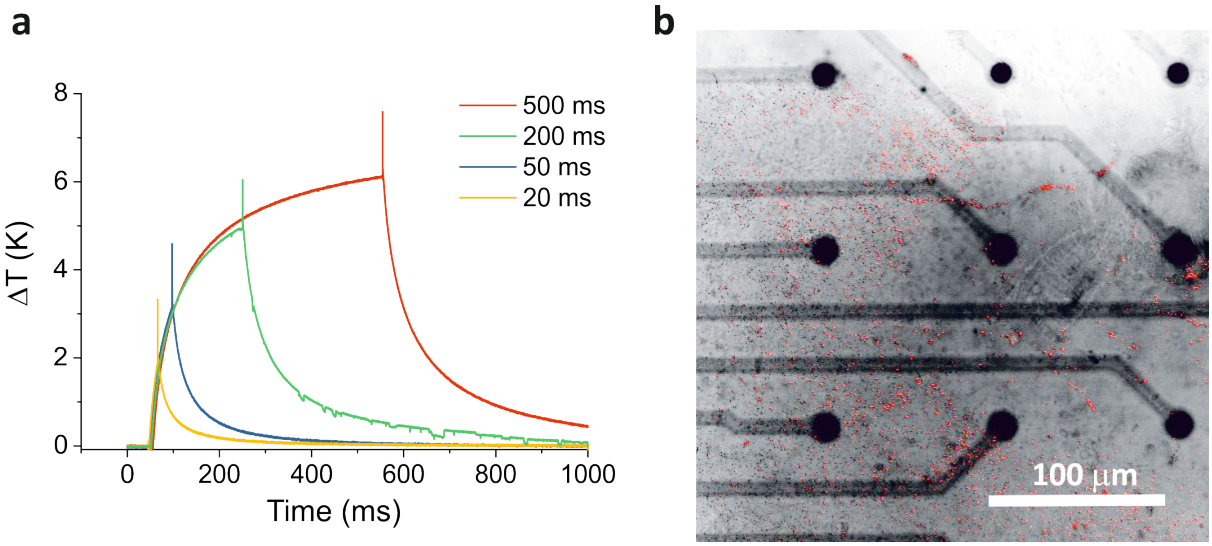

Photothermal effects at the nanoparticle-cell interface. Panel a. Temperature variation (K degrees) as function of time for various durations of light pulses. ***Panel b.*** Fluorescence imaging of P3HT-NP dispersion (red) in an explanted RCS retina layered onto a MEA chip.

To support this concept, we preliminarily simulated the thermal response of NPs dispersed in water using the finite elements method. We considered a volume comparable to the spot of the focused light used for the experiments, which is a 10 µm-high cylinder with area of 0.93 mm^2. In this volume, we simulated randomly dispersed NPs, comparable in number to the density reported for *ex vivo* retinas (~ 3,000 NPs; *panel* ***b***). The NPs are considered as point heat sources that completely convert the absorbed light into heat (for an intensity of 50 mW/mm^2, this amounts to $6.3 \cdot 10^{-9}$ W/NP). In addition, we neglect the reduction of light intensity propagating through the scattering volume. The variation in temperature worked out for this case is below 6 mK, consistent with the above-described experiment. This is not surprising, as a density of 3 x 10^{-4} NPs/μm^3 implies a free volume of about 3,000 μm^3 (a sphere of 9 µm of radius), enough to dissipate the energy when using a CW laser. It is important here to stress that we are using continuous light sources which behave very differently from pulsed sources. Indeed, 50 mW/mm^2 is our peak light intensity, whereas in pulsed lasers the instant power can reach KW/mm^2 or MW/mm^2, which can heat up the particles before they are able to dissipate the energy. Considering that the intensity reaching the retina in our *in vivo* tests is in the order of 10 $\mu W/mm^2$, the thermal effect can be safely ruled out.

Photostimulation mechanism at the nanoparticle-cell interface

P3HT-NPs are light actuators that dwell in close proximity to the neuronal membrane. Upon photoexcitation, generation of negative charges at the polymer/electrolyte surface is taking place. The photo-induced charging of the actuator surface adjacent to the cell membrane is broadly accepted as a source of cell photostimulation [S3-S5].

Surface charge photogeneration. In the biological environment, P3HT is heavily doped by oxygen (p-doping), with an estimated doping concentration up to $1x10^{17}$ cm^{-3}. Photoluminescence is quenched by rapid non-radiative deactivation via energy transfer to charge carriers or electron transfer to oxygen [S6]. Accordingly, the charge separation yield can be high (> 10%). Advanced *ab initio* quantum mechanical calculations show that frontier orbitals (HOMO, LUMO) of the polymer near the interface with the electrolyte downshift in energy due to water molecule polarization, a phenomenon that qualitatively resembles the band bending occurring at Schottky barrier [S7]. Accordingly, negative charges tend to localize at the particle surface due to the interface energy landscape, while holes will diffuse into the bulk, leading to surface polarization. These predictions are consistent with the cathodic behaviour of P3HT in electrochemical cells [S8] and with the negative Z-potential of P3HT-NPs (see **Supplementary Fig. 2**).

Capacitive stimulation. The capacitive mechanism is the accumulation of charges at the particle surface, when no charge transfer reactions are taking place. Only a displacement of ions at the electrode/electrolyte interface takes place, leading to the formation of the double layer at the semiconductor/electrolyte interface.

The capacitive currents may cause cell polarization. A model based on the equivalent circuit can roughly capture the essential features of the nanoparticle-cell coupling. We consider two circuits. The first one is a parallel RC circuit that simulates the charge photogeneration and recombination within the particle. The discharge of this circuit occurs with RC lifetime of 5 ms, in accordance with the estimated lifetime of long-lived polarons in P3HT. The second circuit represents the cell membrane, portioned into junctional and extra-junctional sections. The displacement current across the cleft that eventually polarizes the membrane equals the displacement current flowing through the capacitor of the first circuit. The key parameter that defines the coupling magnitude is the cleft resistance. This is obtained as an average of all possible paths along the NP surface:

$$R_{cleft} \approx \frac{\rho}{2\pi\Delta}\int_{\pi/4}^{\pi/2}\frac{d\emptyset}{sen\emptyset} \cong \frac{\rho}{2\pi\Delta}.$$

Here *r* is the resistivity in the cleft and *D* the cleft thickness (≤ 20 nm, as measured using FIB/SEM investigations). SEM pictures show the engulfment of the neuronal membrane that tightly wraps around the NP, similarly to what has been shown to occur with gold mushroom-electrodes [S9-S11] or nanopillars [S12]. Transmembrane proteins and other macromolecules will further enhance the resistivity of the cleft compared to that of the electrolyte. Accordingly, R_{cleft} can approach 1 GΩ.

For the simulation, we assumed a NP radius of 200 nm and a cleft maximum thickness of 20 nm. We simulated 40 mW/mm^2 light intensity (maximal value used in *in vitro* experiments), 2 eV monochromatic illumination and assumed light be fully absorbed by NPs, with a photon-to-charge conversion efficiency (η) of 10%. $R_{m,j}$ and $C_{m,j}$, represent the resistance and capacitance of the junctional membrane in contact with the cleft, while $R_{m,ej}$ and $C_{m,ej}$ represent the resistance and capacitance of the extra-junctional membrane outside the cleft and exposed to the extracellular electrolyte. These four parameters were calculated by considering the area of the cleft (A_{cleft}) and the area of the cell (A_{cell}), which we assumed 1000 μm^2. The whole cell membrane resistance (R_m) and capacitance (C_m) are assumed being 100 MΩ and 30 pF, respectively. In the case of a single P3HT-NP, $R_{interaction}$ is the in-cleft resistance perpendicular to the junction, calculated by multiplying the resistivity of the electrolyte (assumed to be 100 Ω · cm) by the cleft height and dividing by the cleft area.

The fit parameters reported in **Supplementary Table 1** yielded the junctional and extra-junctional membrane potential changes and the junctional/extra-junctional membrane potential peak variations as a function of the variable cleft resistance reported in **Figure 1h**. The sign of the potential change in the cleft is opposite to the extra-junctional one. Due to the large surface difference between the cleft area and the cell area, voltage changes in the junctional membrane potential will be greatly attenuated in the whole cell membrane potential, as it is the case for postsynaptic potentials in central synapses. Moreover, the effect on the membrane potential scales linearly with the light intensity (set here at about 1-2 orders of magnitude larger than that used in *in vivo* experiments).

Supplementary Table 1. Simulation parameters.

Parameter	Value
Light intensity	4.0 W/cm^2
Photon energy	2 eV
η	0.1
R_{gen}	5 mΩ
$\rho_{electrolyte}$	100 Ω·cm
$r_{nanoparticle}$	200 nm
d_{cleft}	20 nm
$R_{coupling}$	141.543 kΩ
R_{cleft}	7.95775 MΩ
A_{cleft}	0.1413 μm^2
A_{cell}	1000 μm^2
R_{el}	10 Ω
V_m	70 mV
R_m	100 MΩ
C_m	30 pF
$R_{m,j}$	707.714 GΩ
$C_{m,j}$	4.239 fF
$R_{m,ej}$	100.014 MΩ
$C_{m,ej}$	29.9958 pF

SUPPLEMENTARY METHODS

Fabrication of planar P3HT/PET devices. For testing the ability of conductor-less P3HT to stimulate retinal circuits, planar P3HT-only devices were fabricated as previously described [21,23], except that the passive support was PET membrane (Hostaphan® RNK, Mitsubishi Polyester Films, 23 μm nominal thickness) and the deposition of the PEDOT:PSS layer was omitted. Briefly, poly-3-hexylthiophene (P3HT, Sigma Aldrich, 15,000-45,000 molecular weight) solution in chlorobenzene (30 g/l) was deposited on top of a previously rinsed PET membrane by two-steps spin-coating process (800 rpm, 5 s; 1600 rpm, 120 s) followed by a final thermal annealing in glove box (120 °C, 20 min). Retinal implants of suitable dimensions were obtained through laser-assisted cutting, yielding a trapezoid geometry (1.8 mm height, 1.1 mm and 0.55 mm parallel sides) with smoothed edges. Sham PET-only devices underwent the same treatments used in the P3HT annealing protocols, and were cut in the same dimensions using the same laser procedure. Samples were subjected to ethylene oxide sterilization prior to implantation.

Studies in HEK293 cells. Human Embryonic Kidney Cells 293 (HEK293) were obtained from ATCC (CRL-1573). Identity of the cell lines was confirmed by Short Tandem Repeat (STR) profiling. Cells were routinely tested for mycoplasma. HEK293 cells were cultured in cell culture flasks containing Dulbecco's modified Eagle's medium (DMEM) added with 10% Foetal Bovine Serum (FBS), 100 U/ml Penicillin and 100 mg/ml Streptomycin. Culture flasks were maintained in a humidified incubator at 37 °C with 5% CO_2. At 70% confluence, HEK293 cells were enzymatically dispersed using trypsin-EDTA and then plated at a concentration of 15,000 cells/cm^2 for 48 h on Glass- or P3HT-NPs coated coverslips. The hTRPV1-HEK stably transfected clone was employed for the investigation of a possible involvement of TRPV channels in the phototransduction mechanism. The contribution of ASIC channels was investigated in HEK293 cells transiently transfected for hASIC1a-GFP with Lipofectamine 2000. A photo-mediated change in the osmolarity of HEK293 cultured on P3HT- or Glass-NPs was evaluated by a live Calcein-AM staining (Sigma Aldrich). Briefly, 50 μM Calcein-AM solution was added to the cell culture medium and incubated at 37 °C for 30 min in 5% CO_2. The Calcein solution was then removed and cells were washed twice with PBS. Fresh cell culture medium was replaced and cells were imaged by confocal laser scanning microscopy (SP8, Leica Microsystem) with appropriate filter setting using a 40x objective (λ_{ex}, 488 nm; λ_{em}, 500-540 nm), acquired immediately after 500 ms illumination in the absorption spectrum of P3HT (λ_{ex}, 561 nm; λ_{em}, 600-700 nm, and after 12 s in the dark). The cell volume was analysed using Measure_Stack plugin of FIJI (ImageJ).

Studies in primary neurons. Primary cultures of cortical neurons were prepared from embryonic 18-day Sprague-Dawley rat embryos (Charles River). Rats were sacrificed by CO_2 inhalation, and embryos removed immediately by caesarean section. Briefly, the cerebral cortex was dissociated by a 30-min incubation with 0.25 % trypsin at 37 °C and cells were plated on glass coverslips treated with Poly-L-lysine (0.1 mg/ml in borate buffer) in Neurobasal supplemented 2 mM L-glutamine, 2% B27, 100 µg/ml penicillin and 100 µg/ml streptomycin (Life Technologies). P3HT-NPs in saline were added to 14-16 days *in vitro* (DIV) primary neuron cultures to a final concentration of 100 µg/ml. After incubation, neurons were subjected to morphological and electrophysiological examinations. After 1 h of incubation at 37 °C, neurons were stained with the specific membrane dye Cell Mask™ Deep Red Plasma Membrane Stain (λ_{ex}, 633 nm; λ_{em}, 650-750 nm; ThermoFisher) and live imaged at the confocal microscope for the intrinsic P3HT fluorescence (λ_{ex}, 514 nm; λ_{em}, 600-650 nm). Bisbenzimide was employed to highlight nuclei. To monitor NP internalization, neurons exposed to P3HT-NPs for either 1 h or 1 week were fixed, double immunostained for βIII-tubulin and the specific lysosomal marker LAMP1 and analysed by confocal microscopy and ImageJ software to assess colocalization. Alternatively, glass coverslips were coated with a mixture of Poly-L-lysine (0.1 mg/ml in borate buffer) together with glass- or P3HT-NPs (0.4 mg/ml). Primary neurons cultured on P3HT-NPs were live imaged after Calcein-AM staining (SigmaAldrich) as detailed above.

Patch-clamp recordings. *HEK293 cells.* Whole-cell patch-clamp recordings of hTRPV1-HEK and hASIC1a-GFP cells layered on NPs-coated coverslips. The extracellular solution contained (in mM): 135 NaCl, 5.4 KCl, 1 $MgCl_2$, 1.8 $CaCl_2$, 5 HEPES, 10 glucose adjusted to pH 7.4 with NaOH. All recorded cells were brought to a V_h of -70 mV by current injection. hASIC1a were selected on the basis of GFP expression. hTRPV1 channel activity was blocked using 10 µM Capsazepine (Tocris) and hASIC1a channel activity was blocked using 100 µM Amiloride (Tocris).

HEK293 and Retinal Ganglion Cells. All patch-clamp recordings were performed at room temperature using borosilicate patch pipettes (3.5-5.0 MΩ) and under GΩ patch seal, using an EPC10 amplifier (HEKA Elektroniks). The intracellular solution contained (in mM): 126 K-Gluconate, 4 NaCl, 1 $MgSO_4$, 0.02 $CaCl_2$, 0.1 EGTA, 10 Glucose, 5 Hepes, 3 ATP-Na_2, and 0.1 GTP-Na. Light stimulation during electrophysiological experiments was provided by a Lumencor LED system (Spectra X) fibre-coupled to an upright Nikon FN1 microscope (Tokyo, Japan). The light source emission peaked at 530 nm to match the P3HT peak absorption spectrum at 40 mW/mm^2, as measured at the output of the microscope objective. Electrophysiological responses to 500 ms light-pulses were amplified, digitized at 10 or 20

kHz and stored with a Patchmaster V2.73 (HEKA Elektronik). FitMaster v2x90.1 (HEKA Elektronik) was employed for data analysis, together with Prism 6.07 (GraphPad) and OriginPro 9 (OriginLab).

Retina immunohistochemistry.

Photoreceptor cell body counting. (i) Definition of ONL by isolectin GS-IB4 staining and counting of photoreceptor nuclear rows labelled by bisbenzimide. The ONL boundaries were defined based on the blood vessel staining with isolectin GS-IB4 and the number of photoreceptor cell rows was calculated by tracing a radial line through the ONL and counting the number of intersecting bisbenzimide-labelled nuclei using ImageJ. This operation was repeated at least three times for each acquired image. *(ii) Size separation of photoreceptor and bipolar cell bodies labelled by recoverin.* In the rat retina, recoverin labels both rods and cones in the ONL, together with ON and OFF cone bipolar cells in the inner nuclear layer [S13,S14]. The separation between these two layers is evident only in non-dystrophic retinas, while it may create ambiguities in the dystrophic ones. Therefore, to distinguish bipolar cells from photoreceptors in the dystrophic groups, we classified cells based on their major and minor axis using an automated Matlab (MathWorks) support vector machine (SVM) classifier. We trained the classifier using the data collected on the healthy RCS-rdy retinas, where photoreceptors (50 photoreceptors per field) and bipolar cells (all the visible cells) are easily segregated based on their layer position, and then we used the trained classifier to sort all the labelled cells in the dystrophic groups. The misclassification rate was estimated to be 0.53% and 2.13% on the 30 and 240 DPI training dataset, respectively. *(iii) Counting of recoverin, rhodopsin, and cone-arrestin labelled photoreceptor cell bodies.* In non-dystrophic animals, we counted the number of labelled cells in a 50x50 μm region of the ONL scaling it to the total ONL area, while in dystrophic groups, we manually counted all the labelled cells in each field.

Fluorescence density and colocalization analysis. The quantitative analysis of GFAP and FGF2 was performed on the whole retina section using the ImageJ software (NIH). The integrated density of Iba-1 staining was measured on maximum intensity projections of 50-μm z-stack. Colocalization analysis between P3HT- or Glass-NPs with GFAP and Iba-1 was performed on 50 μm z-stacks using the ImageJ JACoP plugin. Random fluorescence overlap was evaluated by rotating the images by 90°.

Surgical injection procedures. Three months-old RCS rats of either sex were anesthetized with an intraperitoneal injection of diazepam (10 mg/kg) followed by intramuscular administration of xylazine (5 mg/kg) and ketamine (33 mg/kg). The subretinal injection of NPs was carried out as follows. A *limbus*-parallel conjunctiva dissection was performed with scissors

for about 2 clock hours in the superior temporal quadrant. A small incision (about 0.5 mm) through the sclera and the choroid was carried out 1 mm from the *limbus*. Then, the retina was gently separated from the retinal pigment epithelium close to the incision using a small amount of viscoelastic material. Glass- or P3HT-NPs (10-20 µl; 1 mg/ml) were then injected through a 38-gauge needle connected to a Hamilton syringe driven by a microinjection apparatus, paying attention to penetrate the subretinal space at the level of the viscoelastic material and to keep the needle tangential to the choroid in order to promote a circular flow that could detach the whole retina. The scleral incision was subsequently coagulated with diathermy and the conjunctiva was gently repositioned over the scleral wound. Surgical procedures were carried out in a sterile room using a Leica ophthalmic surgical microscope. During the whole procedure, the cornea was kept wet. At the end of the intervention, the status of the retina was evaluated by indirect ophthalmoscopy. Antibiotic and corticosteroid eye-drops were applied to prevent inflammation and/or infection after the surgical procedure.

***In vivo* imaging of the retinal implant.** Rats were anaesthetized with isofluorane (3% induction; 2% maintenance in O_2) and their pupils dilated with 1% tropicamide eye drops before image acquisition. Confocal scanning laser ophthalmoscopy (cSLO) was performed with a commercially available scanning-laser ophthalmoscope. Optical coherence tomography (OCT) was performed using the Spectralis™ HRA/OCT device. Each two-dimensional B-Scan recorded at 30° field of view consisted of 1536 A-Scans were acquired at a speed of 40,000 scans/s. Imaging was performed using the proprietary software package Eye Explorer (version 3.2.1.0). The combination of laser scanning retinal imaging and OCT allowed a real-time tracking of eye movements and real-time averaging of OCT scans, thus considerably reducing speckle noise in the OCT images.

RNA Preparation and real-time PCR Analysis. Total RNA was extracted from retina slices with Trizol (Invitrogen, Carlsbad, CA, USA) according to the manufacturer's instructions, purified using RNeasy MinElute Cleanup Kit (Qiagen, Hilden, Germany), and reverse transcribed into cDNA using the SuperScript IV First-Strand Synthesis System (Invitrogen). Gene expression was measured by quantitative real-time PCR (qRT-PCR) using the CFX96 Touch Real-Time PCR Detection System (BioRad). Relative gene expression was determined using the 2-ΔΔCT method [S15]. *Gapdh* and *Hprt1* were used as reference genes. The list of the used primers is provided in **Supplementary Table 2**.

Supplementary Table 2. List of the primers and their description.

Gene Symbol	Description	Forward sequence	Reverse sequence
Opn1sw	opsin 1, short wave sensitive	ACGTTCTGGTCAATGTAT	CCAAAGAGGAAGTATCCAT
Opn1mw	opsin 1, medium wave sensitive	CCACTATCTACAATCCCATT	CTATCATCAACTTTCTTTCCAA
Gapdh	glyceraldehyde-3-phosphate dehydrogenase	CCATTCTTCCACCTTTGA	CTGTAGCCATATTCATTGTC
Hprt1	hypoxanthine phosphoribosyltransferase 1	TGGATATGCCCTTGACTAT	ACAGGACTCTTGTAGATTCA
Rho	rhodopsin	CCCTCAGTGTTCTTTTCT	GATGGATGTCCTTTGTCA

Positron emission tomography (PET) imaging. Rats were kept under fasting conditions with free access to water for 6 h and anesthetized by the intraperitoneal administration of diazepam (4 mg/kg) followed by intramuscular administration of ketamine/xylazine (5 mg/kg and 33 mg/kg, respectively). Serum glucose level was tested soon before the intravenous injection of 37-74 MBq ^{18}F-FDG through the tail vein. Animals, positioned on the bed of a dedicated micro-PET system kept at 5 lux, were subjected to light flash stimulation (5 lux corneal irradiation; 0.5 Hz) for 40 min followed by 10 min static scan acquisition. PET data were reconstructed using a maximal likelihood expectation maximization method (MLEM). An experienced observer in double blind conditions identified a volume of interest in the primary visual cortex (V1; ~1 mm^3) using RMI brain scans and stereotaxic coordinates [S16], to measure the average standardized uptake value (SUV). This value represents the most commonly accepted index of ^{18}F-FDG retention and represents tracer uptake as the fraction of injected tracer dose normalized for body weight [44,S17].

Statistics and Reproducibility. The results of the statistical tests performed on the experimental data throughout the study are reported as exact *p* values in **Supplementary Table 3.**

Supplementary Table 3. Statistical analysis and exact *p* values.

FIGURE NUMBER	*TEST USED*	*n*	*p VALUE*	*DEGREES OF FREEDOM & F/t/z/R/ETC VALUE*
			I - Interaction, G - Group	
1d	Wilcoxon's one-tailed test	5 RGCs from 5 rats	0.0313	NA
1e	two-way ANOVA/Fisher's LSD test	P3HT-NPs: 35, 55, 112, 224 neurons/21 retinas; Glass-NPs: 25, 38, 83, 167 neurons/18 retinas; Control: 21, 44, 91, 192/19 retinas; for 1, 7, 18, 40 mW/mm^2 stimuli, respectively	I, G: 0.0012, 0.0436/for 1, 7, 18, 40 mW/mm^2 - 0.4590,0.5153,0.0113, <0.0001	I, G: F (3, 751) = 5.353, F (1, 751) = 4.084
1f	Student's two-tailed *t*-test	52 neurons/15 non-injected RCS-rdy retinas and 207 neurons/10 RCS-injected retinas	<0.0001	t=12.18 df=256
2a	Kolmogorov-Smirnov test	6 RCS rats per each experimental group	0.4005	D = 0.4
2b	Mann-Whitney two-tailed *U*-test	*same as* ***b***	top, bottom: 0.3939, 0.3268	U = 12, 11.5
2c	Kolmogorov-Smirnov test, Mann-Whitney two-tailed *U*-test	*same as* ***b***	left, right: 0.4005, 0.6991	D = 0.4, U = 15
3a	one-way ANOVA/Tukey's test	RCS-rdy, RCS, RCS+P3HT and RCS+Glass: 5, 5, 5, 4 rats	<0.0001/RCS-rdy vs all groups - <0.0001	F (3, 15) = 256.7
3b	one-way ANOVA/Tukey's test	RCS-rdy, RCS, RCS+P3HT and RCS+Glass: 4, 4, 4, 4 rats,	<0.0001/RCS-rdy vs all groups - <0.0001	F (3, 12) = 728.0
3c	one-way ANOVA/Tukey's test	RCS-rdy, RCS, RCS+P3HT and RCS+Glass: 4, 6, 7, 11 rats,	<0.0001/RCS-rdy vs all groups - <0.0001	F (3, 24) = 149.6
3d	one-way ANOVA/Tukey's test	RCS-rdy, RCS, RCS+P3HT and RCS+Glass: 5, 5, 5, 4 rats	<0.0001/RCS-rdy vs all groups - <0.0001	F (3, 15) = 86.46
3e	one-way ANOVA/Tukey's test	RCS-rdy, RCS, RCS+P3HT and RCS+Glass: 3, 4, 4, 4 rats	<0.0001/RCS-rdy vs all groups - <0.0001	F (3, 11) = 256.1
3f	one-way ANOVA/Tukey's test	RCS-rdy, RCS, RCS+P3HT and RCS+Glass: 4, 4, 4, 4 rats	<0.0001/RCS-rdy vs all groups - <0.0001	F (3, 12) = 238.9
4b	repeated measures ANOVA	RCS-rdy, RCS, RCS+P3HT and RCS+Glass: 8, 11, 24, 18 rats	<0.0001/RCS vs RCS-rdy @3.5, 5, 7, 10, 15, 20 lux - 0.0002, 0.0014, 0.0032, 0.0006, 0.002, 0.0002, RCS+P3HT vs RCS+Glass all <0.0001	F (3,57)=34.26
4c	repeated measures ANOVA	RCS-rdy, RCS, RCS+P3HT and RCS+Glass: 7, 6, 6, 8 rats	<0.0001/RCS vs RCS-rdy @3.5, 5, 7, 10, 15, 20 lux - 0.0219, 0.0123, 0.0177, 0.0031, 0.0013, 0.0033, RCS+P3HT vs RCS+Glass @3.5, 5, 7, 10, 15, 20 lux - 0.0263, 0.0104, 0.0052, 0.0015, 0.0172, 0.0077	F (3,23)=16.16
4d	one-way ANOVA/Tukey's test	*same as* ***b*** *and* ***c***	<0.0001/RCS-rdy 30DPI vs RCS 30DPI 0.0004, RCS-rdy 30DPI vs RCS+Glass 30DPI 0.0004, RCS-rdy 240DPI vs RCS 240DPI 0.0009, RCS-rdy 240DPI vs RCS+Glass 240DPI 0,0002, RCS 30DPI vs RCS+P3HT 30DPI 0.0003, RCS 240DPI vs RCS+P3HT 240DPI 0.0004, RCS+P3HT 30DPI vs RCS+Glass 30DPI 0.0002, RCS+P3HT 240DPI vs RCS+Glass 240DPI 0.0002	F (7,80)=26.40

5c	one-way ANOVA/Tukey's test	RCS-rdy, RCS, RCS+P3HT and RCS+Glass: 8, 7, 12, 6 rats	<0.0001/RCS-rdy vs RCS 0.003, RCS-rdy vs RCS+P3HT 0.014, RCS-rdy vs RCS+Glass 0.0007, RCS vs RCS+P3HT 0.006, RCS vs RCS+Glass 0.9501, RCS+P3HT vs RCS+Glass 0.0006	F (3,29)=28.11
5d	one-way ANOVA/Tukey's test	RCS-rdy, RCS, RCS+P3HT and RCS+Glass: 10, 10, 6, 7 rats	<0.0001/RCS-rdy vs RCS 0.0007, RCS-rdy vs RCS+P3HT 0.1776, RCS-rdy vs RCS+Glass 0.0009, RCS vs RCS+P3HT 0.0008, RCS vs RCS+Glass 0.8382, RCS+P3HT vs RCS+Glass 0.0006	F (3,29)=160.3
5e	one-way ANOVA/Tukey's test	RCS-rdy, RCS, RCS+P3HT and RCS+Glass: 4, 4, 4, 4 rats	<0.0001/RCS-rdy vs RCS 0.009, RCS-rdy vs RCS+P3HT 0.0371, RCS-rdy vs RCS+Glass 0.0008, RCS vs RCS+P3HT 0.023, RCS vs RCS+Glass 0.999, RCS+P3HT vs RCS+Glass 0.021	F (3,12)=22.19
5f	one-way ANOVA/Tukey's test	*same as* ***e***	<0.0001/RCS-rdy vs RCS 0.0001, RCS-rdy vs RCS+P3HT 0.372, RCS-rdy vs RCS+Glass 0.0003, RCS vs RCS+P3HT 0.0002, RCS vs RCS+Glass 0.5827, RCS+P3HT vs RCS+Glass 0.0002	F (3,12)=26.43
5h	one-way ANOVA/Tukey's test	RCS-rdy, RCS, RCS+P3HT and RCS+Glass: 8, 4, 7, 4 rats	<0.0001/RCSrdy W vs RCS W < 0.0001, RCSrdy W vs RCS+P3HT W 0.0005, RCSrdy W vs RCS+GlassF W < 0.0001, RCS W vs RCS+P3HT W 0.0007, RCS+P3HT RED vs RCS+P3HT W 0.008, RCS+P3HT W vs RCS+GlassF W 0.0006	F (11,55)=124.6
6b	one-way ANOVA/Tukey's test	RCS-rdy, RCS, RCS+P3HT and RCS+Glass: 12, 10, 24, 10 rats	<0.0001/RCS-rdy vs RCS 0.007, RCS-rdy vs RCS+P3HT 0.8484, RCS-rdy vs RCS+Glass 0.0087, RCS vs RCS+P3HT 0.0007, RCS vs RCS+Glass 0.9999, RCS + P3HT vs RCS+Glass 0.0009	F (3,52)=15.19
6c	one-way ANOVA/Tukey's test	*same as****b***	<0.0001/RCS-rdy vs RCS 0.0004, RCS-rdy vs RCS+P3HT 0.7722, RCS-rdy vs RCS+Glass 0.0003, RCS vs RCS+P3HT 0.0009, RCS vs RCS+Glass 0.5139, RCS+P3HT vs RCS+Glass 0.0008	F (3,52)=23.71
6d	one-way ANOVA/Tukey's test	RCS-rdy, RCS, RCS+P3HT and RCS+Glass: 7, 9, 8, 8 rats	<0.0001/RCS-rdy vs RCS 0.0002, RCS-rdy vs RCS+P3HT 0.9882, RCS-rdy vs RCS+Glass 0.0059, RCS vs RCS+P3HT 0.0007, RCS vs RCS+Glass 0.346, RCS+P3HT vs RCS+Glass 0.0038	F (3,28)=16.31
6e	one-way ANOVA/Tukey's test	*same as* ***d***	<0.0001/RCS-rdy vs RCS 0.0004, RCS-rdy vs RCS+P3HT 0.9988, RCS-rdy vs RCS+Glass 0.0001, RCS vs RCS+P3HT 0.0003, RCS vs RCS+Glass 0.7567, RCS+P3HT vs RCS+Glass 0.0002	F (3,28)=23.61
S1	one-way ANOVA/Tukey's test	RCS-rdy, RCS, RCS+P3HT and RCS+Glass: 6, 6, 7, 5 rats	<0.0001/RCS-rdy vs RCS 0.0002, RCS-rdy vs RCS+(P3HT+PET) 0.0071, RCS-rdy vs RCS+PET 0.0002, RCS vs RCS+(P3HT+PET) 0.0025, RCS vs RCS+PET 0.9802, RCS+(P3HT+PET) vs RCS+PET 0.0034	F (3,20)=40.60

S3a	Student's two-tailed *t*-test	8 cells from 2 independent preparations	0.4102	t = 0.8456 df = 16
S3b	Mann-Whitney's *U*-test	4 cells from 2 independent preparations	0.4857	U = 5
S4c	one-way ANOVA/Tukey's test	10 coverslips from 2 independent preparations	0.7011/>0.7 for all multiple comparisons	F = 0.4764
S5a	Wilcoxon matched-pairs signed rank test, paired Student's *t*-test, Wilcoxon matched-pairs signed rank test	P3HT-NPs, Glass-NPs, No injection - 10, 9, 7 retinal explants from at least 5 animals	0.3750, 0.7274, 0.8438	t = 0.3629 df = 7 (Glass-NPs)
S5b	Wilcoxon's two-tailed test	P3HT-NPs, Glass-NPs, No injection - 5, 4, 5 retinal explants from at least 4 animals	0.0625, 0.6250, 0.6250	NA
S7a	two-way ANOVA/Tukey's test	6 rats for both groups	I, G: 0.3265,0.1483/Ventral-Glass vs. Ventral-P3HT 0.4472, Central-Glass vs. Central-P3HT 0.9997, Dorsal-Glass vs. Dorsal-P3HT 0.9145, < 0.4 for all other combinations	I, G: F(2, 30) = 1.162, F(1, 30) = 2.202
S7b	two-way ANOVA/Tukey's test	6 rats for both groups	I, G: 0.3295,0.9130/Ventral-P3HT vs. Ventral-Glass 0.9998, Central-P3HT vs. Central-Glass 0.9072, Dorsal-P3HT vs. Dorsal-Glass 0.8787, < 0.4 for all other combinations	I, G: F(2, 30) = 1.152, F(1, 30) = 0.01215
S7c	Kolmogorov-Smirnov	P3HT, Glass - 4, 6 RCS rats	left to right: 0.41752, 0.78693, 0.78693	D = 0.4, 0.3, 0.3
S8a	two-way ANOVA/Tukey's test	P3HT, Glass - 4, 6 RCS rats	I, G: 0.2704, 0.3311/Central-P3HT vs. Central-Glass 0.9385, Ventral-P3HT vs. Ventral-Glass 0.6976, Dorsal-P3HT vs. Dorsal-Glass 0.9718, >0.2 for all other combinations	I, G: F(2, 22) = 1.686, F(1, 22) = 0.6935
S8b	Mann-Whitney's two-tailed *U*-test	same as ***a***	0.3524	U = 7
S8c	two-way ANOVA/Tukey's test	P3HT, Glass - 4, 5 RCS rats	I, G: 0.7264, 0.8324/Central-P3HT vs. Central-Glass 0.995, Ventral-P3HT vs. Ventral-Glass 0.9911, Dorsal-P3HT vs. Dorsal-Glass 0.9996, >0.6 for all other combinations	I, G: F(2, 21) = 0.3112, F(1, 21) = 0.04271
S8d	Mann-Whitney's two-tailed *U*-test	same as ***c***	>0.9999	U = 10
S13b	one-way ANOVA/Tukey's test	RCS-rdy, RCS, RCS+P3HT and RCS+Glass: 12, 10, 24, 10 rats	0.6885/RCS-rdy vs RCS 0.9955, RCS-rdy vs RCS+P3HT 0.727, RCS-rdy vs RCS+Glass 0.8085, RCS vs RCS+P3HT 0.8923, RCS vs RCS+Glass 0.9215, RCS+P3HT vs RCS+Glass > 0.9999	F (3,52)=0.4933
S13c	one-way ANOVA/Tukey's test	RCS-rdy, RCS, RCS+P3HT and RCS+Glass: 7, 9, 8, 8 rats	0.6822/RCS-rdy vs RCS 0.9983, RCS-rdy vs RCS+P3HT 0.6314, RCS-rdy vs RCS+Glass > 0.9999, RCS vs RCS+P3HT 0.69, RCS vs RCS+Glass 0.9981, RCS+P3HT vs RCS+Glass 0.6056	F (3, 28) = 0.7088
S16a	Mann-Whitney's two-tailed *U*-test	P3HT-NPs, Glass-NPs - 6, 5 rats	0.0823	U = 5
S16c	Mann-Whitney's two-tailed *U*-test	30DPI, 240DPI - 6, 5 rats	0.9307	U = 14

E1c	Mann-Whitney's two-tailed *U*-test	22 neurons from 2 independent cultures	0.5885	U = 218.5
E2b	one-way ANOVA/Bonferroni's test	RCS-rdy, RCS, RCS+P3HT, RCS+Glass - 13,13,11,14 rats	< 0.0001/RCS-rdy vs all groups - <0.0001	F (3, 47) = 263.5
E2d	one-way ANOVA/Bonferroni's test	RCS-rdy, RCS, RCS+P3HT, RCS+Glass - 9,9,8,10 rats	< 0.0001/RCS-rdy vs all groups - <0.0001	F (3, 32) = 240.6
E4a	one-way ANOVA /Newman-Keuls test	4 rats for each experimental group	*30 DPI* - < 0.001/RCS-rdy vs all groups *240 DPI* - < 0.001/RCS-rdy vs all groups	*30 DPI* - F (3, 12) = 23,92 *240 DPI* - F (3, 12) = 89,83
E4b	one-way ANOVA /Newman-Keuls test	4 rats for each experimental group	*30 DPI* - < 0.001/RCS-rdy vs all groups *240 DPI* - RCS-rdy vs. RCS 0.001, RCS-rdy vs. RCS+P3HT 0.003, RCS-rdy vs. RCS+Glass 0.006	*30 DPI* - F (3, 12) = 455.0 *240 DPI* - F (3, 12) = 8.86
E4c	one-way ANOVA /Newman-Keuls test	4 rats for each experimental group	*30 DPI* - < 0.001/RCS-rdy vs all groups *240 DPI* - < 0.001/RCS-rdy vs all groups	*30 DPI* - F (3, 12) =69.77 *240 DPI* - F (3, 12) = 39.44
E5a	one-way ANOVA/Dunnett's test	RCSrdy, RCS, RCS+P3HT, RCS+Glass - 11, 10, 10, 11 rats	<0.0001/RCS-rdy vs all groups - <0.0001	F (3, 38) = 17.96
E5b	one-way ANOVA/Dunnett's test	RCSrdy, RCS, RCS+P3HT, RCS+Glass - 11, 12, 12, 12 rats	<0.0001/RCS-rdy vs all groups - <0.0001	F (3, 43) = 20.19
E5c	one-way ANOVA/Dunnett's test	RCSrdy, RCS, RCS+P3HT, RCS+Glass - 8, 7, 7, 8	0.0002/RCS-rdy vs RCS- 0.0007, RCS-rdy vs P3HT - 0.0009, RCS-rdy vs Glass - 0.0008	F (3, 26) = 9.450
E5d	one-way ANOVA/Dunnett's test	RCSrdy, RCS, RCS+P3HT, RCS+Glass - 7, 6, 6, 7 rats	<0.0001/RCS-rdy vs RCS- 0.0001, RCS-rdy vs P3HT - 0.0005, RCS-rdy vs Glass - <0.0001	F (3, 22) = 12.90
E5e	one-way ANOVA/Dunnett's test	RCSrdy, RCS, RCS+P3HT, RCS+Glass - 8, 9, 8, 8 rats	0.0004/RCS-rdy vs RCS- 0.0133, RCS-rdy vs P3HT - 0.0005, RCS-rdy vs Glass - 0.0015	F (3, 29) = 8.422
E5f	one-way ANOVA/Dunnett's test	RCSrdy, RCS, RCS+P3HT, RCS+Glass - 4, 4, 4, 4 rats	0.0004/RCS-rdy vs RCS- 0.0073, RCS-rdy vs P3HT - 0.0003, RCS-rdy vs Glass - 0.0008	F (3, 12) = 13.16
E6a	one-way ANOVA/Tukey's test	3*0 DPI* - RCSrdy, RCS, RCS+P3HT, RCS+Glass - 8, 7, 12, 6 rats *240 DP*I - RCSrdy, RCS, RCS+P3HT, RCS+Glass - 4, 4, 4, 4 rats	*30 DPI* - <0.0001/RCS-rdy vs RCS 0.0091, RCS-rdy vs RCS+P3HT 0.0099, RCS-rdy vs RCS+Glass 0.0071, RCS vs RCS+P3HT 0.336, RCS vs RCS+Glass 0.999, RCS+P3HT vs RCS+Glass 0.331 *240 DPI* - <0.0001/RCS-rdy vs RCS 0.0002, RCS-rdy vs RCS+P3HT 0.0002, RCS-rdy vs RCS+Glass 0.0002, RCS vs RCS+P3HT 0.514, RCS vs RCS+Glass 0.9979, RCS+P3HT vs RCS+Glass 0.6159	*30 DPI* - F (3,29)=17.48, *240 DPI* - F (3,12)=162.8
E6b	one-way ANOVA/Tukey's test	RCS-rdy, RCS+P3HT- 8, 7 rats	<0.0001/W-RCS+P3HT vs R-RCS+P3HT 0.9934, <0.0001 for all other combinations	F (3,25)=1671
E7b	one-way ANOVA/Tukey's test	RCS-rdy, RCS, RCS+P3HT and RCS+Glass: 10, 12, 14, 11 rats	0.0026/RCS-rdy vs RCS 0.0334, RCS-rdy vs RCS+P3HT 0.9963, RCS-rdy vs RCS+Glass 0.0491, RCS vs RCS+P3HT 0.0096, RCS vs RCS+Glass 0.9745, RCS+P3HT vs RCS+Glass 0.0364	F (3,43)=5.57

Supplementary references

S1. Martino, N. *et al.* Photothermal cellular stimulation in functional bio-polymer interfaces. *Sci Rep* **5**, 8911 (2015).

S2. Lodola, F., Martino, N., Tullii, G., Lanzani, G. & Antognazza, M.R. Conjugated polymers mediate effective activation of the mammalian ion channel transient receptor potential vanilloid 1. *Sci Rep* **7**, 8477 (2017).

S3. Schoen, I. & Fromherz, P. The mechanism of extracellular stimulation of nerve cells on an electrolyte-oxide semiconductor capacitor. *Biophys J* **92**, 1096-1111 (2007).

S4. Parameswaran, R. *et al.* Photoelectrochemical modulation of neuronal activity with free-standing coaxial silicon nanowires. *Nat Nano* **13**, 260-266 (2018).

S5. Srivastava, S.B. *et al.*, Band alignment engineers faradaic and capacitive photostimulation of neurons without surface modification. *Phys Rev Appl* **11**, 044012 (2019).

S6. Bellani, S. *et al.* Reversible P3HT/oxygen charge transfer complex identification in thin films exposed to direct contact with water. J *Phys Chem C* **118**, 6291-6299 (2014).

S7. Mosconi, E. *et al.* Surface polarization drives photo-induced charge separation at the P3HT/Water interface. *ACS Energy Lett* **1**, 454-463 (2016).

S8. Lanzarini, E. *et al.* Polymer-based photocatalytic hydrogen generation. *J Phys Chem C* **116**, 10944-10949 (2012).

S9. Fendyur, A., Mazurski, N., Shappir, J. & Spira, M.E. Formation of essential ultrastructural interface between cultured hippocampal cells and gold mushroom-shaped MEA - toward "IN-CELL" recordings from vertebrate neurons. *Front Neuroeng* **4**, 14 (2011).

S10. Shmoel, N. *et al.* Multisite electrophysiological recordings by self-assembled loose-patch-like junctions between cultured hippocampal neurons and mushroom-shaped microelectrodes. *Sci Rep* **6**, 27110 (2016).

S11. Ojovan, S.M. *et al.* A feasibility study of multisite, intracellular recordings from mammalian neurons by extracellular gold mushroom-shaped microelectrodes. *Sci Rep* **5**, 14100 (2015).

S12. Hanson, L., Lin, Z.C., Xie, C., Cui, Y. & Cui, B. Characterization of the cell-nanopillar interface by transmission electron microscopy. *Nano Lett* **12**, 5815-5820 (2012).

S13. Milam, A.H., Dacey, D.M. & Dizhoor, A.M. Recoverin immunoreactivity in mammalian cone bipolar cells. *Vis. Neurosci.* **10**, 1-12 (1993).

S14. Günhan, E., Van der List, D. & Chalupa L.M. Ectopic photoreceptors and cone bipolar cells in the developing and mature retina. *J. Neurosci*. **23**, 1383-1389 (2003).

S15. Vandesompele, J. *et al.* Accurate normalization of real-time quantitative RT-PCR data by geometric averaging of multiple internal control genes. *Genome Biol.* **3**, RESEARCH0034 (2002).

S16. Paxinos, G. & Watson, C. *The rat brain in stereotaxic coordinates.* Vol. 6. Elsevier Inc. (2007).

S17. Marini, C. *et al.* Direct inhibition of hexokinase activity by metformin at least partially impairs glucose metabolism and tumour growth in experimental breast cancer. *Cell Cycle* **12**, 3490-3499 (2013).

SUPPLEMENTARY FIGURES

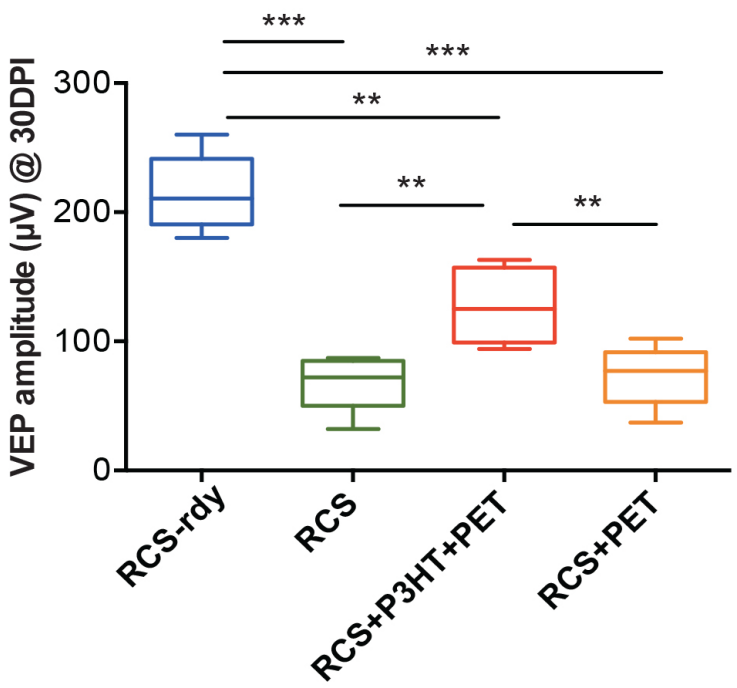

Supplementary Fig. 1: Rescue of light-evoked visual responses in RCS rats implanted with a planar P3HT-only device. The amplitude of VEP recordings in V1 in response to flash stimuli (20 cd m^{-2}; 200 ms; 1 Hz) shows the rescue of light sensitivity in implanted dystrophic RCS rats at 30 days post implantation (DPI) with respect to non-implanted (RCS) or sham-implanted (RCS+PET) rats and to healthy congenic controls (RCS-rdy). The full device consisted in P3HT layered on PET, while the sham-device was PET only. One-way ANOVA/Tukey's tests: ** $p<0.01$; *** $p<0.001$. Box plots represent the median (centre line), mean (square), (animals): RCS-rdy, n=6; RCS, n=6; RCS+P3HT implant, n=7; RCS+Sham implant, n=5. For exact p values, see **Supplementary Table 3.**

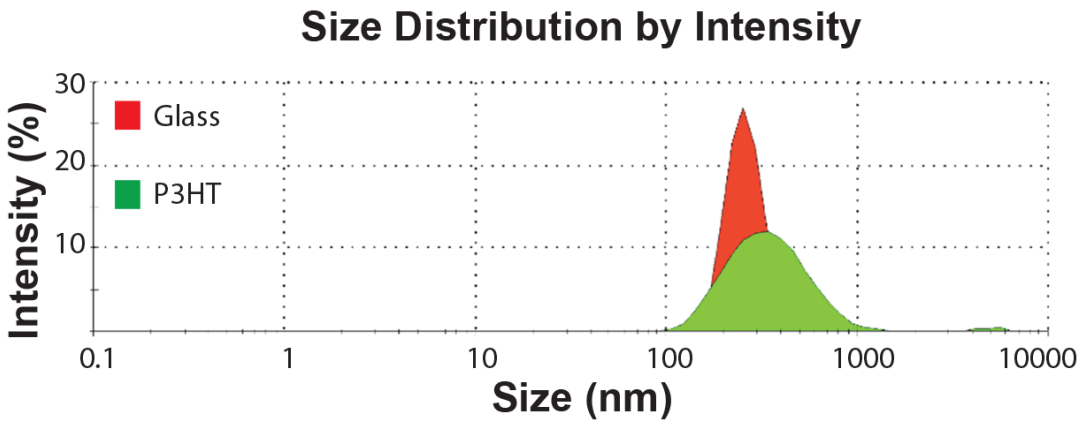

Material	Z-Average (nm)	St. Dev.	PDI
Glass	254	± 52	0.043
P3HT	304	±176	0.222

Supplementary Fig. 2: Characterization of P3HT- and glass nanoparticles. Size distribution of Glass- and P3HT-NPs was determined by dynamic light scattering (DLS) analysis. The results are representative of n=3 independent NP preparations.

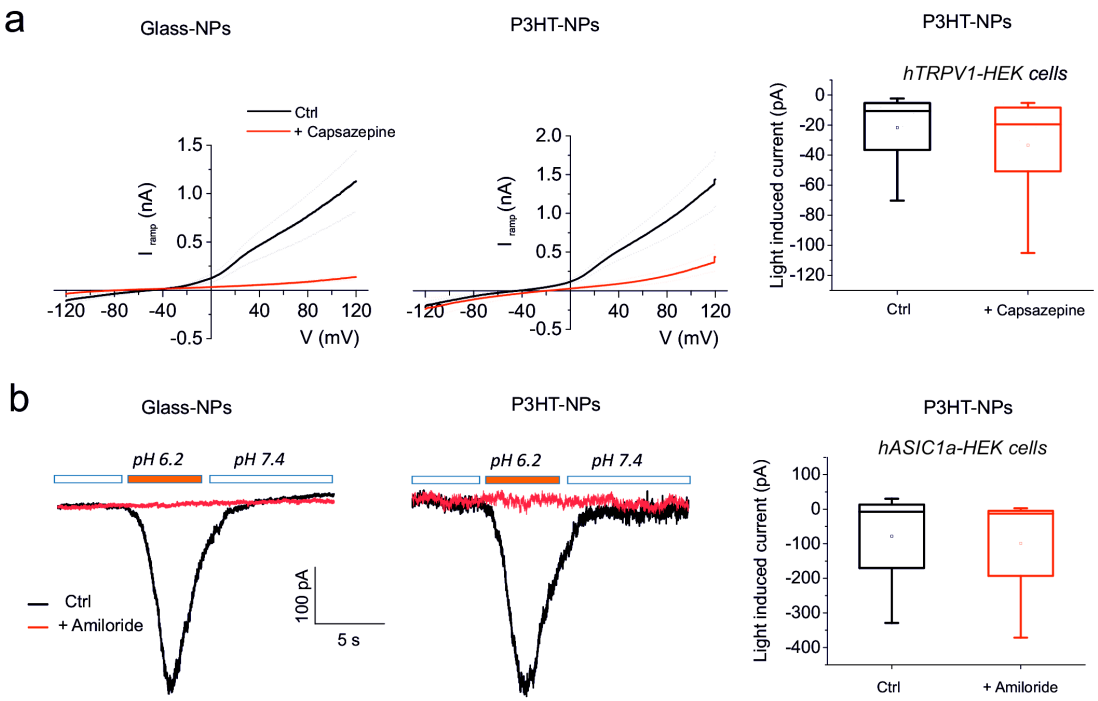

Supplementary Fig. 3: Light-evoked membrane depolarization by P3HT nanoparticles cells does not involve TRPV and ASICs channels in HEK293. (a) I/V curves of hTRPV1 stably transfected HEK293 cells on coverslips treated with either Glass- or P3HT-NPs showing the inhibition of the hTRPV1-mediated current by capsazepine (10 μM; *left*). The analysis of the light-induced current for the P3HT-NPs group before and after the application of the drug revealed no effects of the hTRPV1 blockade in the photostimulation (*right*, n=8 from at least 2 independent preparations). **(b)** Representative voltage-clamp traces showing inward currents in hASIC1a transiently transfected HEK293 cells in response to a decrease in pH that are completely inhibited by amiloride (100 μM; *left*). The analysis of the light-induced current for the P3HT-NPs group before and after the application of amiloride revealed no effects of the hASIC1a blockade (*right*, n = 4 from at least 2 independent preparations). Box plots represent the median (centre line), mean (square), 25th-75th percentiles (box) and the limit of 3-fold the interquartile range.

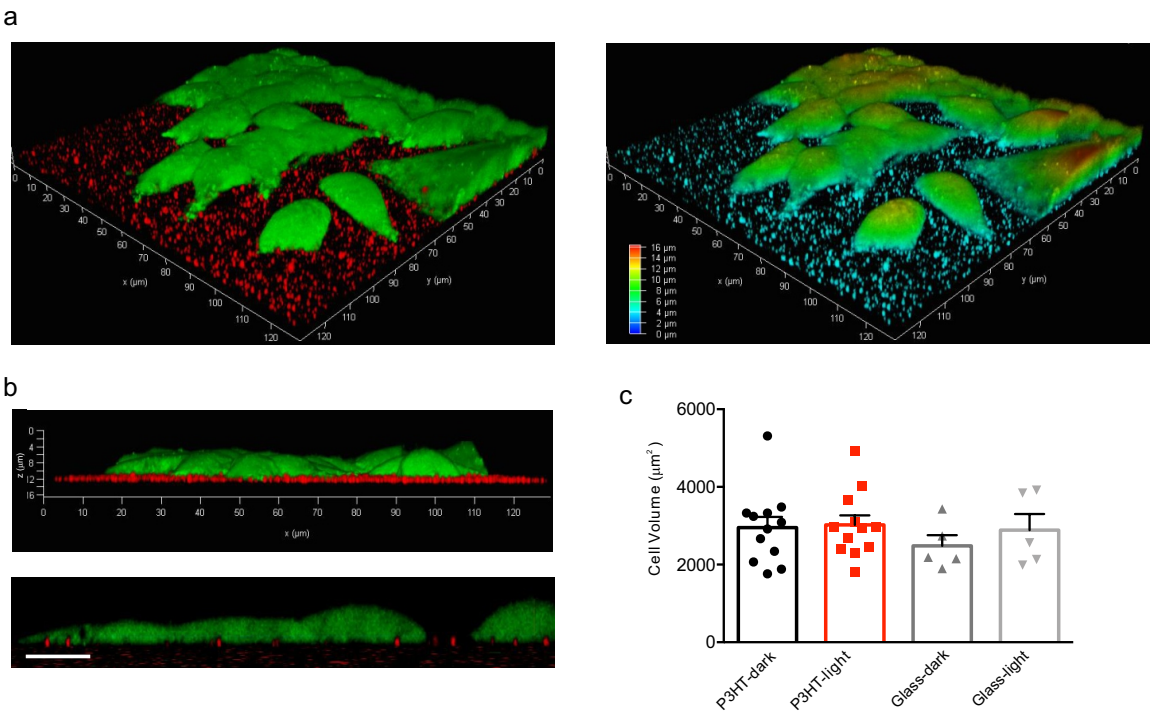

Supplementary Fig. 4: P3HT nanoparticles do not induce osmolality changes in HEK293 cells upon illumination. (a) 3D reconstruction of a z-stack confocal imaging of HEK293 cells cultured on coverslips coated with P3HT-NPs. *Left:* Calcein-AM staining (green) and P3HT fluorescence (red). *Right:* False-colour image of the cell profile height along the z-axis. **(b)** The xz-projection of the sections along the y-axis shows that NPs on the coverslip are not internalized into the cell bodies (top), also confirmed by a representative xz-section (bottom; scale bar, 10 µm). **(c)** The quantification of the confocal stacks obtained by time-lapse Calcein-AM fluorescence acquisitions shows no effects of P3HT-NPs photo-stimulation on the cell body volume. Data are means±sem with superimposed individual experimental points. Sample size: n = 10, from 2 independent preparations.

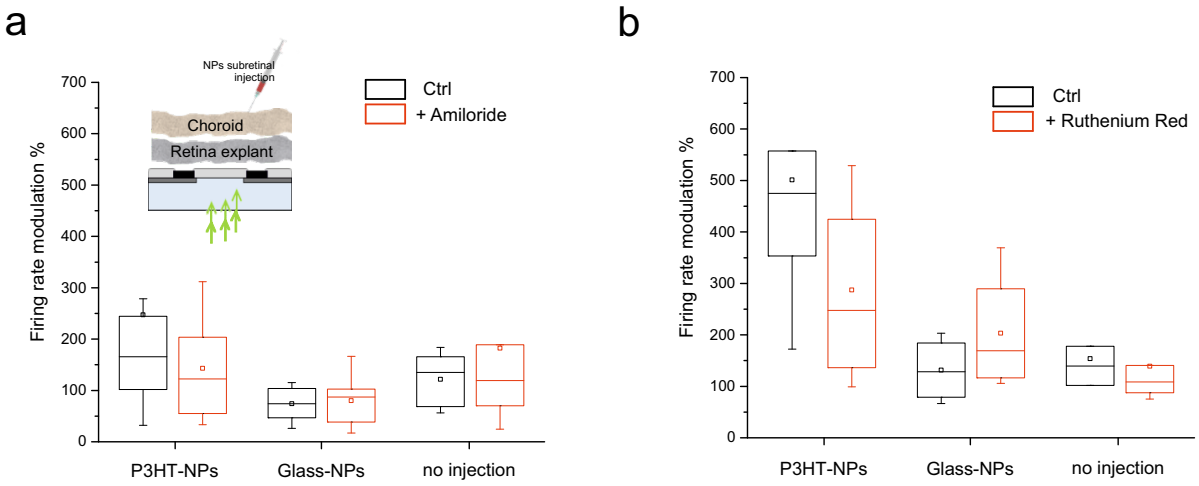

Supplementary Fig. 5: Light-evoked membrane depolarization by P3HT nanoparticles in blind RCS retina explants does not involve TRPV and ASICs channels. (a) Modulation of RGC firing activity recorded extracellularly on MEAs (epiretinal electrode configuration) by green light pulses before and after administration of amiloride (100 µM) in retinal explants from 12-16 months-old RCS rats injected subretinally with either glass or P3HT NPs. The results show no difference among the groups, confirming that ASICs channels are not involved in the fast modulation of retinal activity. Sample size: n = 10, 9 and 7 retinal explants for P3HT-NPs, Glass-NPs and Ctrl, respectively, from 5 individual animals. **(b)** A similar experiment was carried out using Ruthenium Red (10 µM) to block TRPV channels, showing no role of such channels in the photo-transduction mechanism by P3HT-NPs with neurons. Sample size: n = 5, 4 and 5 retinal explants for P3HT-NPs, Glass-NPs and Ctrl, respectively, from 4 individual animals. All the experiments used 500 ms light pulses at 540 nm, 40 mW/mm^2 at 0.25 Hz. Box plots represent the median (centre line), mean (square), 25th-75th percentiles (box) and the limit of 3-fold the interquartile range.

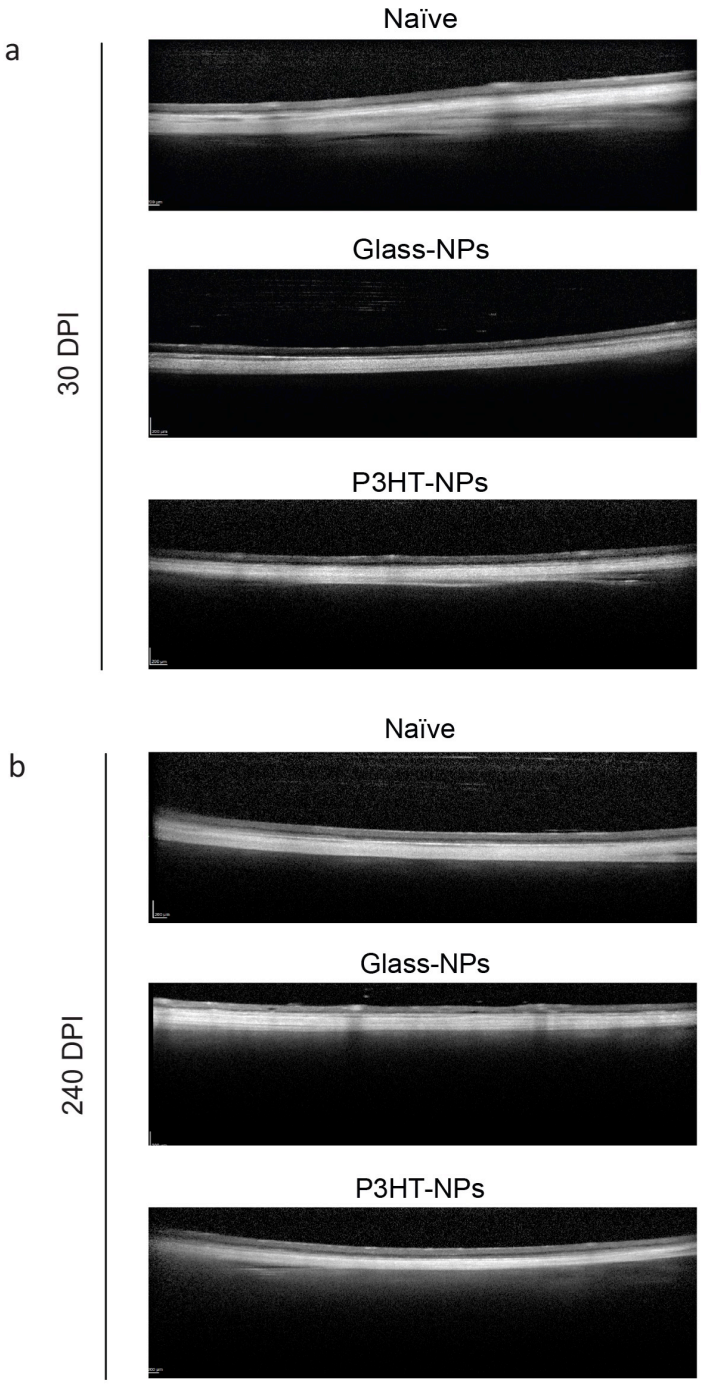

Supplementary Fig. 6: Ocular coherence tomography of nanoparticle-microinjected RCS retinas at 30 and 240 DPI. Representative ocular coherence tomography pictures of the eye of dystrophic RCS rats that were non-injected (naïve) or injected with either control glass-NPs or P3HT-NPs. *In vivo* eye imaging was performed at 30 **(a)** and 240 **(b)** DPI in all injected dystrophic RCS rat with closely similar results. No retinal detachments, breakages or signs of inflammation were observed. Since the trans-scleral microinjection did not touch the retina, no signs of injection are visible.

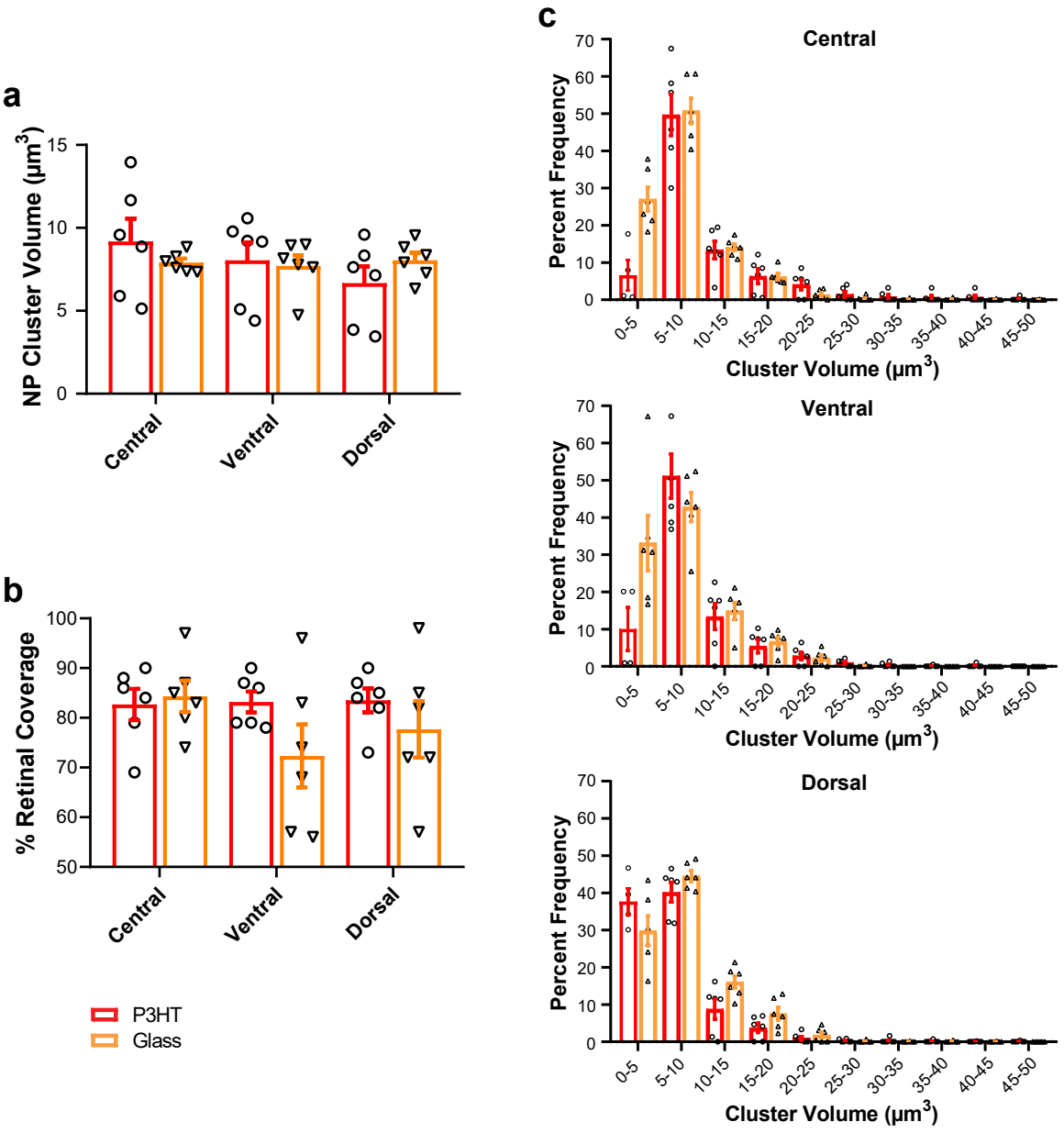

Supplementary Fig. 7: Regional characterization of nanoparticle distribution at 30 DPI. **(a)** Mean volume of P3HT- (red) and Glass-NP clusters (yellow) in the central, ventral and dorsal regions of the retina. p>0.05 P3HT *vs* Glass, two-way ANOVA/Tukey's tests. **(b)** Subretinal space coverage by P3HT- (red) and Glass- (yellow) NPs in the central, ventral and dorsal regions of the retina. p>0.05 P3HT *vs* Glass, two-way ANOVA/Tukey's tests. **(c)** Frequency distribution (% of total clusters) of the size of P3HT- and Glass-NP clusters in the central, ventral and dorsal sections of the retina (5 µm bins). The coverage and volume distribution are similar in all retinal districts for both treatments. Bar plots represent means ± sem with superimposed individual experimental points. Sample size: n=6 animals for both experimental groups. For exact p values, see **Supplementary Table 3.**

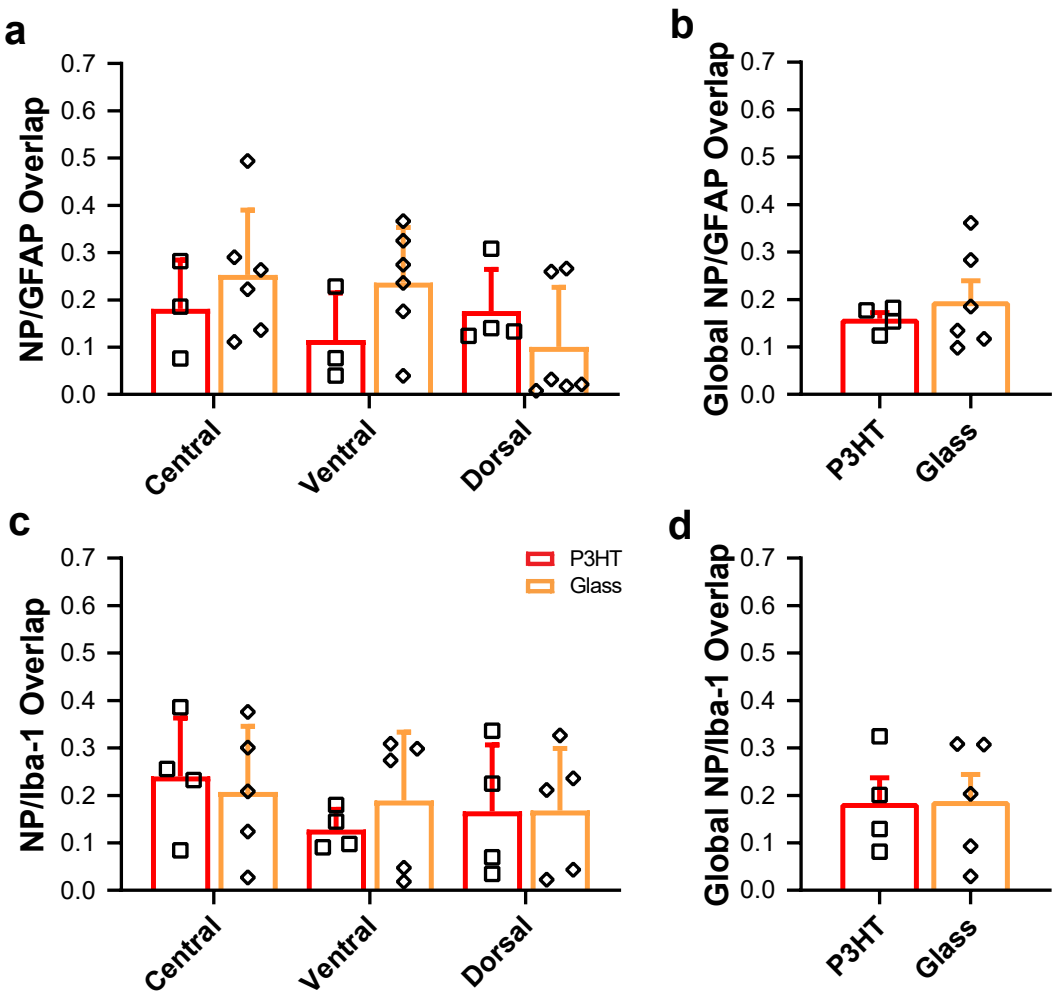

Supplementary Fig. 8: Overlap between injected nanoparticles and the expression of pro-inflammatory markers in the RCS retina at 30 DPI. NP/Antibody colocalization analysis was performed on 50-µm z-stack sections of dystrophic RCS rat retinas injected with either P3HT-NPs (red bars) or fluorescent Glass-NPs (orange bars) and stained for the astrocyte/Müller cell marker GFAP **(a,b)** and the microglial marker Iba-1 **(c,d).** In each retinal section, images were acquired from the corresponding central, ventral and dorsal districts (2-3 sections per animal) and analysed with ImageJ. The extent of overlap was evaluated using the Manders' M1 coefficient, defined as the extent of above-threshold fluorescence simultaneously present in both the NP and Antibody channels, normalized to the NP channel alone (ranging between 0 for full signal segregation and 1.0 corresponding to full signal overlap). Data (means ± sem with superimposed individual experimental points) are expressed as the difference between the Manders' M1 coefficient calculated from the pristine image and the one mirrored for the NP fluorescence channel. Regional distribution of the Manders' overlap coefficient **(a,c)** and retina averages, calculated per each animal **(b,d).** Both treatments showed very low levels of overlap between inflammatory markers and NP fluorescence. $p>0.05$, two-way ANOVA **(a,c)**; $p>0.05$, Mann-Whitney *U*-test **(b,d)**. Sample size (experimental animals): GFAP, n=4 and 6; Iba-1, n= 4 and 5; for P3HT-NPs and Glass-NPs, respectively. For exact p values, see **Supplementary Table 3.**

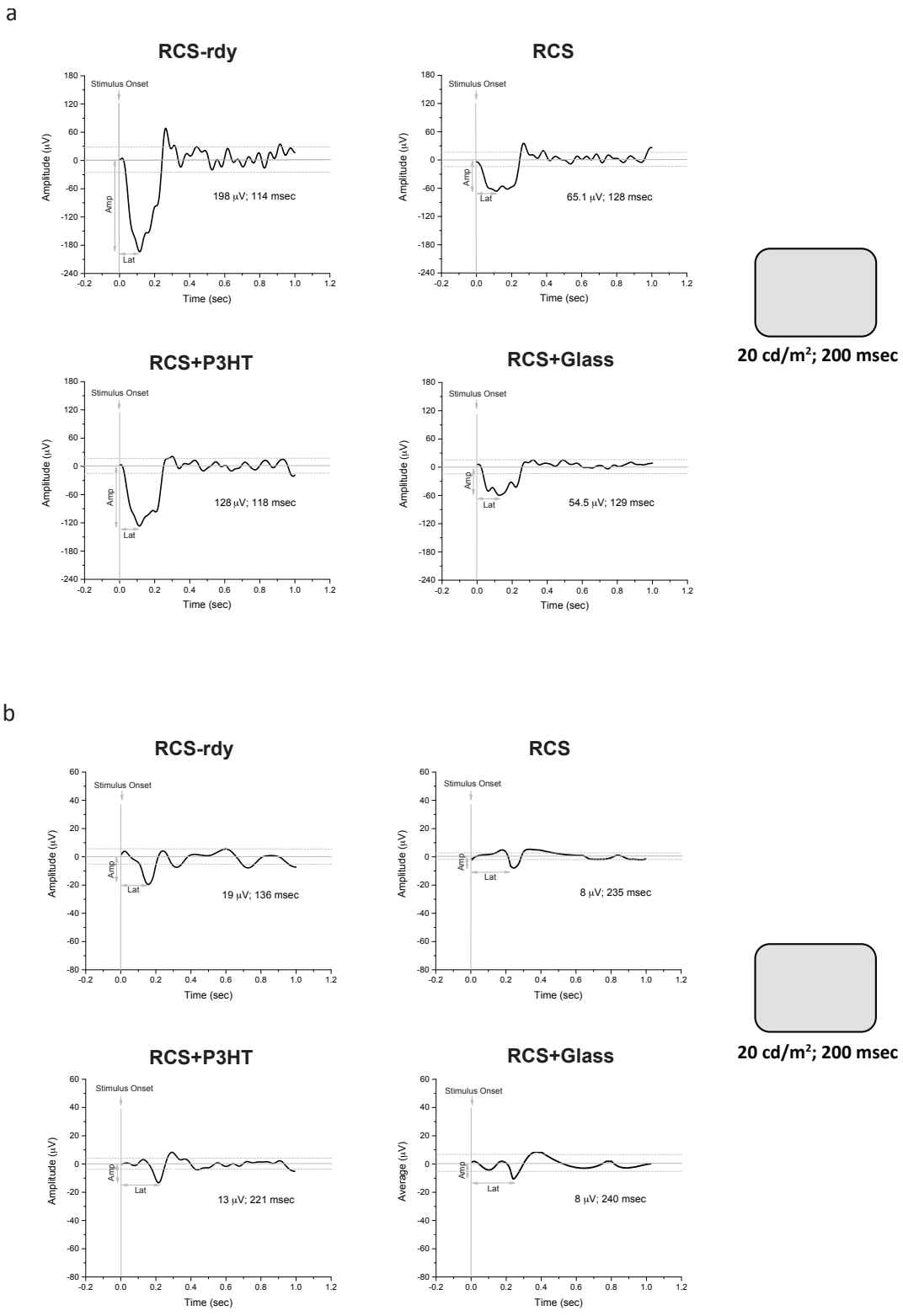

Supplementary Fig. 9: VEP recordings in response to flash stimuli. Representative traces of VEPs evoked by flash stimuli (20 cd/m^2, 200 ms) of white light (400-700 nm) recorded at 30 **(a)** and 240 **(b)** DPI in the four experimental groups (RCS-rdy; RCS; RCS+P3HT-NPs; RCS+Glass-NPs). Traces are the average of 50 sweeps. The peak detection algorithm collects potentials above 2 x SD of the noise (dashed horizontal lines on both sides of the baseline) and gives latencies from stimulus onset and peak-to-baseline amplitudes.

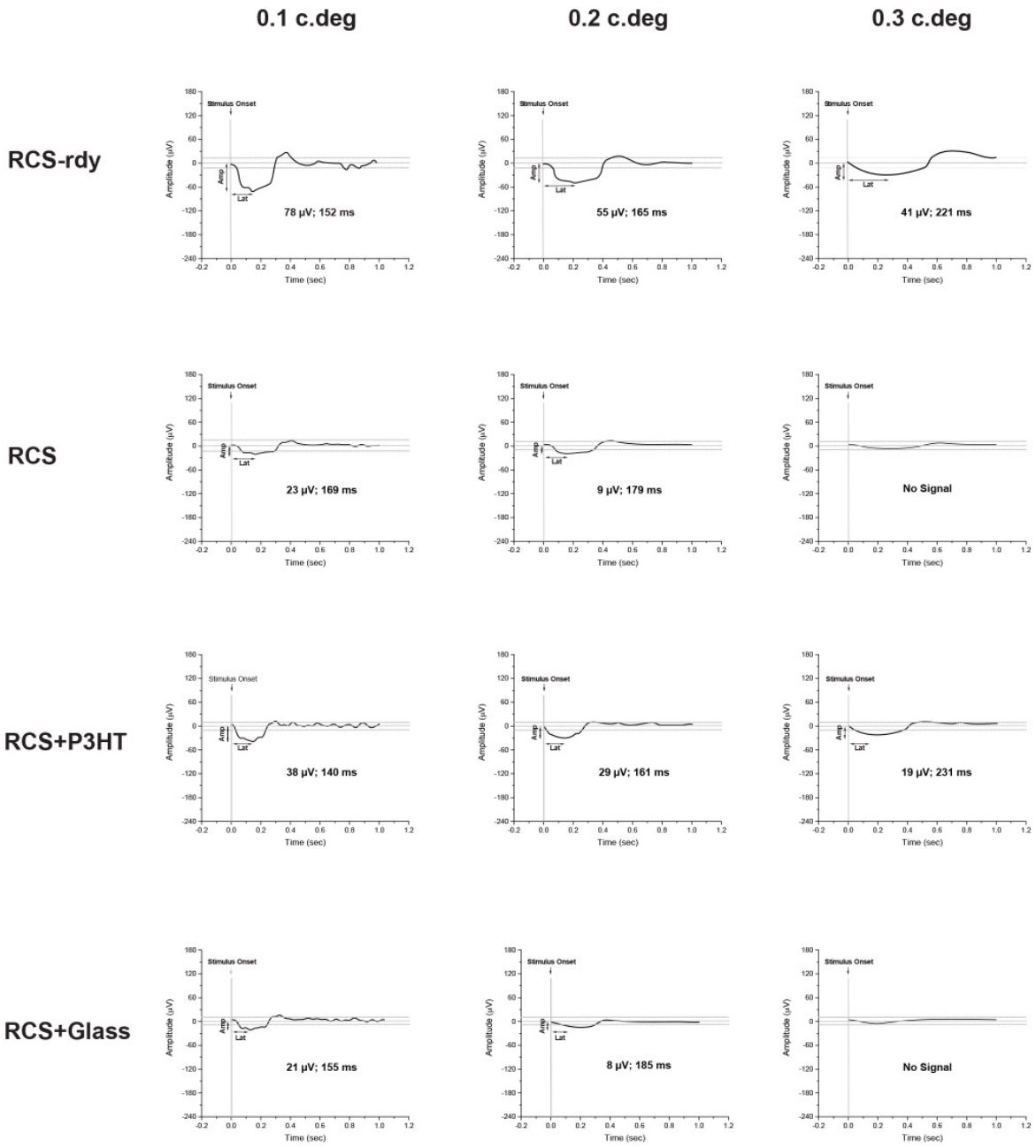

Supplementary Fig. 10: VEP recordings in response to patterned stimuli. Representative traces of VEPs evoked by patterned stimuli of increasing spatial frequency (20 cd/m^2, 0.1-0.3 cycles/degree) recorded at 30 DPI in the four experimental groups (RCS-rdy; RCS; RCS+P3HT-NPs; RCS+Glass-NPs). Traces are the average of 50 sweeps. The peak detection algorithm collects potentials above 2 x SD of the noise (dashed horizontal lines on both sides of the baseline) and gives latencies and peak-to-baseline amplitudes.

a

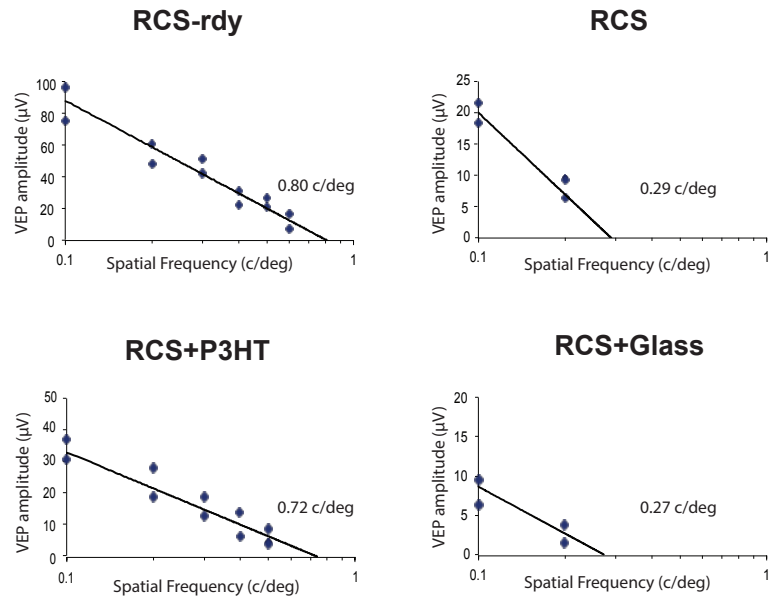

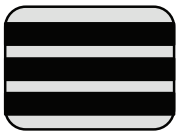

Pattern stimuli / SF
20 cd/m²; 1 Hz

b

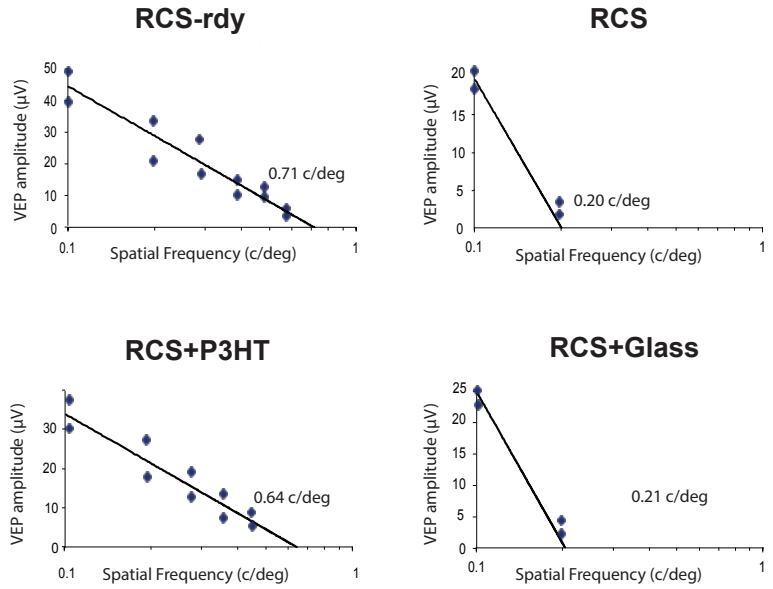

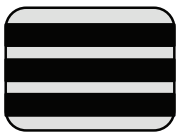

Pattern stimuli / SF
20 cd/m²; 1 Hz

Supplementary Fig. 11: Analysis of visual acuity. Determination of visual acuity in representative animals at 30 **(a)** and 240 **(b)** DPI from the four experimental groups (RCS-rdy; RCS; RCS+P3HT-NPs; RCS+Glass-NPs) by using patterned visual stimuli (20 cd/m^2@1.0 Hz) of varying spatial frequency (0.1-1 cycle/degree). VEP amplitude values were plotted *vs* the log of spatial frequency and a linear regression was computed on the decreasing VEP amplitudes before plateauing. Visual acuity was then estimated as the X-intercept of the regression line.

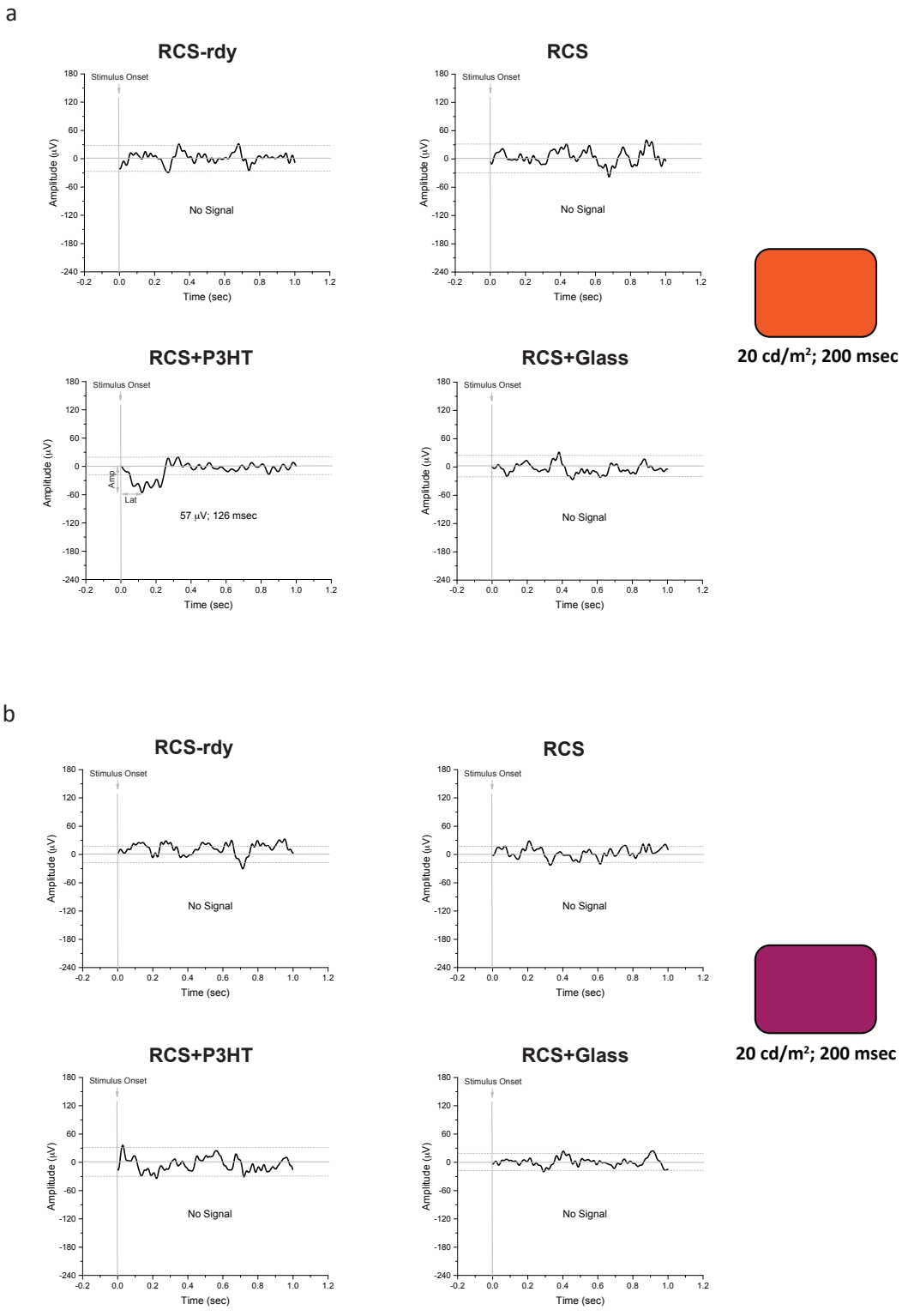

Supplementary Fig. 12: VEP recordings in response to red and infrared flash stimuli. Representative traces of VEPs evoked by flash stimuli (20 cd/m^2, 200 ms) of red light (**a**; 575-700 nm) or near-infrared light (**b**; 750-800 nm) recorded at 30 DPI in the four experimental groups (RCS-rdy; RCS; RCS+P3HT-NPs; RCS+Glass-NPs). Traces are the average of 50 sweeps. The peak detection algorithm collected potentials above 2 x SD of noise (dashed horizontal lines on both sides of the baseline) to yield latency and amplitude values.

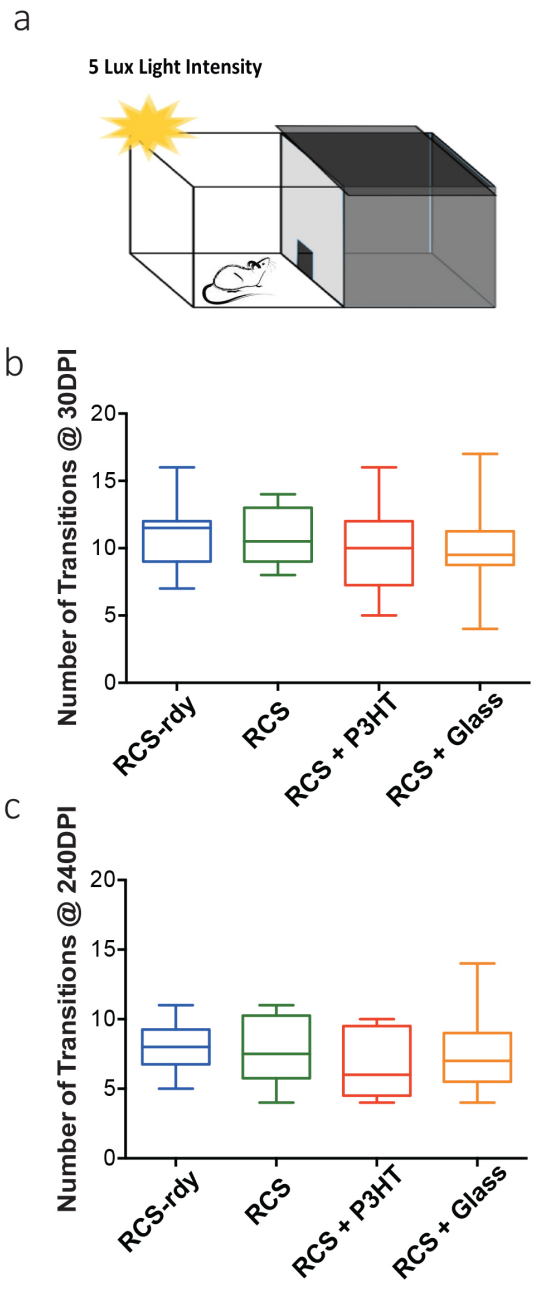

Supplementary Fig. 13: Number of transitions in the light-dark box test. (a) Schematics of the light-dark box test. **(b,c)** The number of transitions between the light and dark compartments over the 6 min of video-recording was evaluated in the four experimental groups (RCS-rdy; RCS; RCS+P3HT-NPs; RCS+Glass-NPs) and used as an index of light-independent motor activity. No differences were observed among the experimental groups at both 30 **(b)** and 240 (**c**) DPI. Box plots represent the median (centre line), 25th-75th percentiles (box) and the limit of 3-fold the interquartile range. p>0.05 one-way ANOVA/Tukey's tests. Sample size (animals): RCS-rdy, n=12 and 7; RCS, n=10 and 9; RCS+P3HT-NPs, n=24 and 8; RCS+Glass-NPs, n=10 and 8, for 30 and 240 DPI, respectively. For exact p values, see **Supplementary Table 3.**

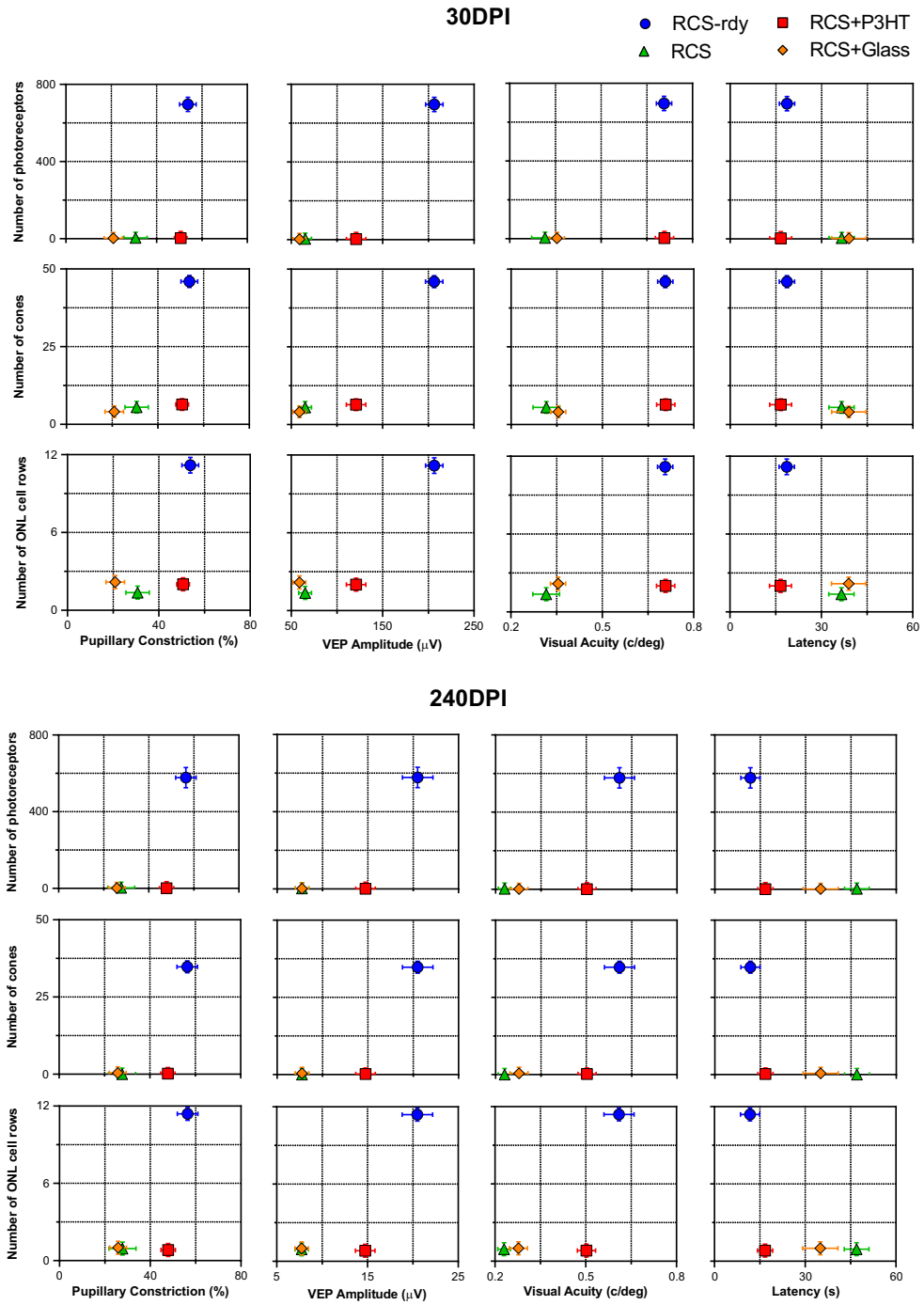

Supplementary Fig. 14: Correlation between functional performances and photoreceptor cell body populations in individual animals at 30 and 240 DPI. A subpopulation of RCS rats underwent the complete panel of functional and histopathologic analyses. The correlation plots depict the means ± sem of the individual values of photoreceptor cell body counts (recoverin-stained photoreceptor cell bodies, cone arrestin-positive cone cell bodies and bisbenzimide-stained ONL cell rows) and visual performances (pupillary constriction, VEP amplitude, visual acuity and escape latency) for the four experimental groups. 30 DPI: RCS-rdy (blue; n=5), RCS (green; n=5), RCS+P3HT-NPs (red; n=5) and RCS+Glass-NPs (orange; n=6). 240 DPI: RCS-rdy (blue; n=4), RCS (green; n=4), RCS+P3HT-NPs (red; n=4) and RCS+Glass-NPs (orange; n=4).

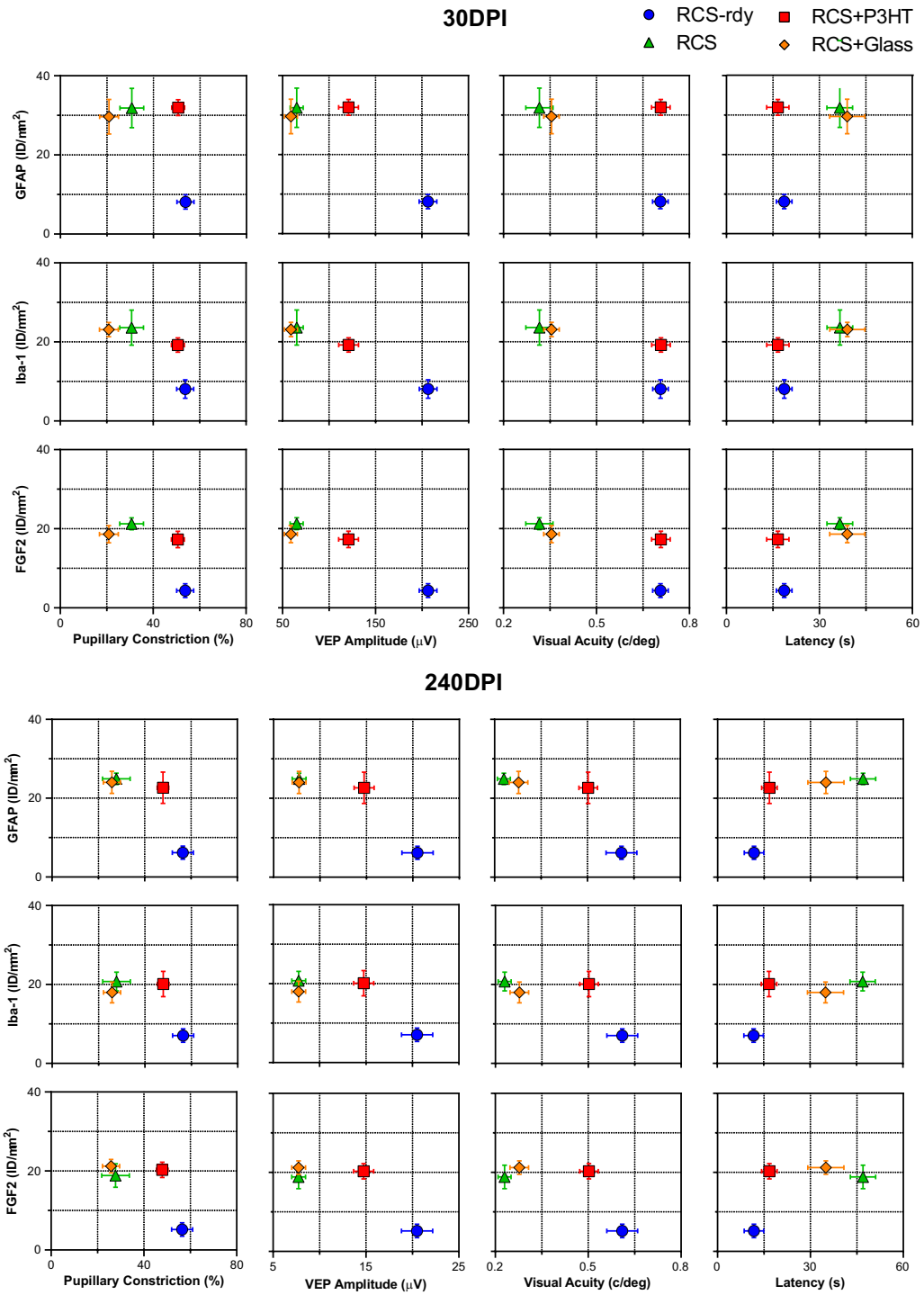

Supplementary Fig. 15: Correlation between functional performances and pro-inflammatory/trophic markers in individual animals at 30 and 240 DPI. A subpopulation of RCS rats underwent the complete panel of functional and histopathologic analyses. The correlation plots depict the means ± sem of the individual values for pro-inflammatory/trophic markers (GFAP, Iba-1 and FGF2) and visual performances (pupillary constriction, VEP amplitude, visual acuity and escape latency) for the four experimental groups. 30 DPI: RCS-rdy (blue; n=5), RCS (green; n=5), RCS+P3HT-NPs (red; n=5) and RCS+Glass-NPs (orange; n=6). 240 DPI: RCS-rdy (blue; n=4), RCS (green; n=4), RCS+P3HT-NPs (red; n=4) and RCS+Glass-NPs (orange; n=4).

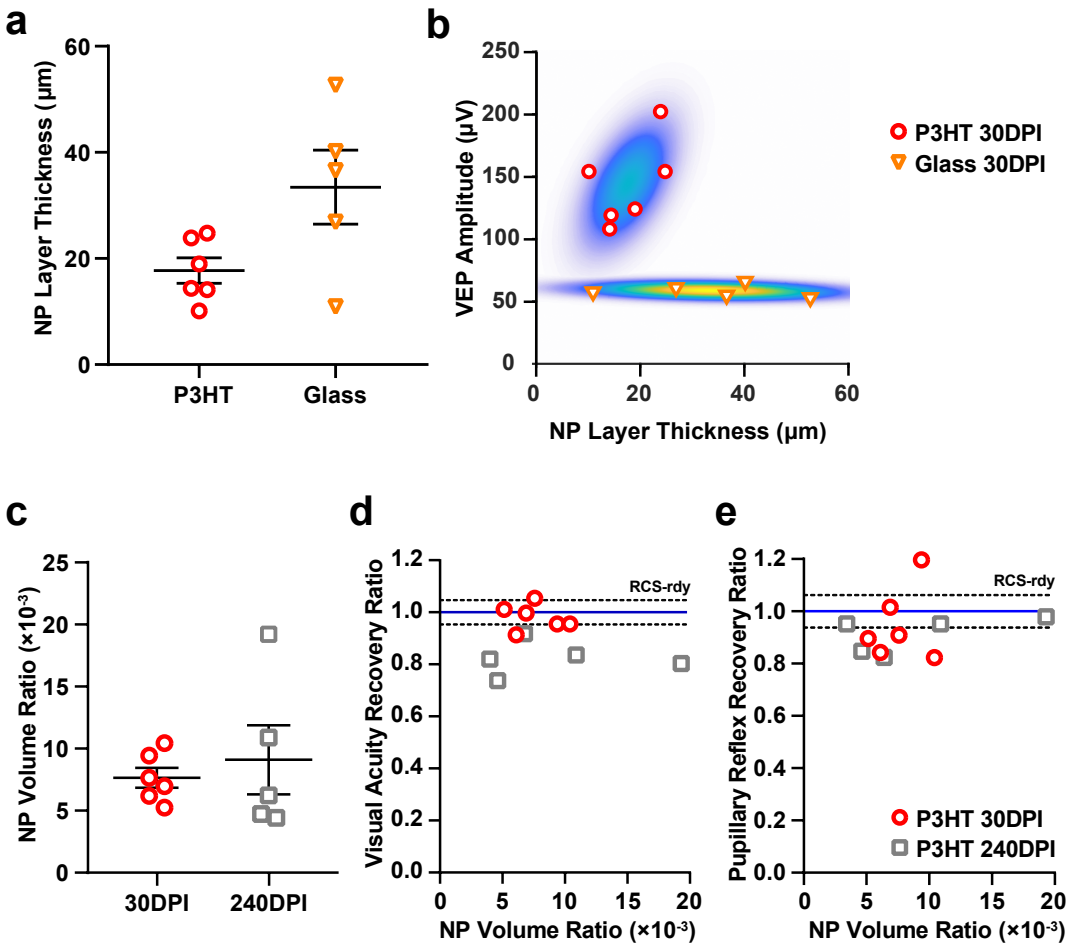

Supplementary Fig. 16: Reproducibility of the NP layer thickness and NP volume ratio in the ONL *vs* visual performances. (a) Thickness of the P3HT-NP and fluorescent Glass-NP layer measured at 30 DPI along transversal sections of RCS retinas using confocal microscopy. Data are means±sem with superimposed individual experimental points. p>0.05, Mann-Whitney *U*-test. Sample size: n=6 and 5 animals for P3HT-NPs and glass-NPs, respectively. **(b)** Relationships between thickness of the NP layer and VEP amplitude in response to flash stimuli in dystrophic RCS rats injected with either P3HT-NPs (red symbols; n=6 animals) or fluorescent Glass-NPs (yellow symbols; n=5 animals) at 30 DPI. To test for discrete clustering between the Glass- and P3HT-NP groups, a Matlab macro was used to fit a two-component Gaussian mixture model on unlabelled data and losslessly re-cluster it into the two experimental groups. **(c)** The total volume occupied by P3HT-NP clusters in the ONL (NP volume ratio) was obtained for RCS rats at 30 and 240 DPI by dividing the cluster volume of P3HT-NPs (see Fig. 2) by the estimated volume of the ONL measured using z-stack confocal analysis and the ImageJ software. Data are means±sem with superimposed individual experimental points. p>0.05, Mann-Whitney *U*-test. Sample size: n= 6 and 5 animals for 30 and 240 DPI, respectively. **(d,e)** Relationships between the NP volume ratio and the visual performance of dystrophic RCS rats injected with P3HT-NPs at either 30 (red symbols; n=6 animals) or 240 (grey symbols; n=5 animals) DPI evaluated as visual acuity (**d**) and pupillary reflex (**e**) performances normalized by the respective mean RCS-rdy values. The solid and broken horizontal lines in the plot represent the mean (± sem) visual performance of healthy RCS-rdy rats.

Captions to Supplementary Movies

Movie S1. Pupillary reflexes in bilaterally injected and dark-adapted animals at 30 DPI evoked by a light stimulus of 5 lux. Movies are image sequences obtained with a Hamamatsu camera at 5 Hz frame rate. Representative examples of the four experimental groups (RCS-rdy; RCS; RCS+P3HT-NPs; RCS+Glass-NPs) are shown.

Movie S2. Pupillary reflexes in bilaterally injected and dark-adapted animals at 240 DPI evoked by a light stimulus of 5 lux. For further details, see caption to Movie S1.

Movie S3. Escape latency in the light-dark box test at 30 DPI. A representative example of the light (5 lux)-evoked escape behavior is shown for each experimental group (RCS-rdy; RCS; RCS+P3HT-NPs; RCS+Glass-NPs).

Movie S4. Escape latency in the light-dark box test at 240 DPI. For further details, see caption to Movie S3.